

# Lower mantle composition and temperature from mineral physics and thermodynamic modelling

E. Mattern,<sup>1</sup> J. Matas,<sup>1</sup> Y. Ricard<sup>2</sup> and J. Bass<sup>3</sup>

<sup>1</sup>Laboratoire de Sciences de la Terre, CNRS UMR 5570, Ecole normale supérieure de Lyon, 46, allée d'Italie, 69364 Lyon cedex 07, France.

E-mails: estelle.mattern@ens-lyon.fr and jan.matas@ens-lyon.fr

<sup>2</sup>Laboratoire de Sciences de la Terre, CNRS UMR 5570, Université Claude Bernard Lyon1, 43Bd du 11 novembre,

Bat. Géode, 69622 Villeurbanne cedex, France. E-mail: ricard@ens-lyon.fr

<sup>3</sup>Department of Geology, University of Illinois at Urbana-Champaign, Urbana, IL 61801, USA. E-mail: jaybass@uiuc.edu

Accepted 2004 December 8. Received 2004 September 15; in original form 2004 April 25

## SUMMARY

A generalized inverse method is applied to infer the radial lower mantle composition and temperature profile from seismological models of density and bulk sound velocity. The computations are performed for a five-component system, MgO–FeO–CaO–Al<sub>2</sub>O<sub>3</sub>–SiO<sub>2</sub> and three phases: (Mg,Fe,Al)(Si,Al)O<sub>3</sub> perovskite, (Mg,Fe)O magnesiowustite, and CaSiO<sub>3</sub> perovskite. A detailed review of the elasticity data set used to compute the elastic properties of mineral assemblages is given. We consider three different *a priori* compositional models—pyrolite, chondritic and a model based on cosmic abundances of elements—as *a priori* knowledge for the inversions in order to investigate the sensitivity of any given best-fit solution to the assumed initial composition. Consistent features in all inversions, independent of the *a priori* model, are a total iron content of  $X_{\text{Fe}} \simeq 0.10 \pm 0.06$  and a subadiabatic temperature gradient over most of the lower mantle depth range. A peculiar correlated behaviour of the two most sensitive parameters (iron content and temperature) is found below the 660 km discontinuity: over the depth range from 660 km down to 1300 km. Significantly, we find that the bulk composition inferred from any given inversion is strongly dependent on the choice of *a priori* model. Equally satisfactory fits to the lower mantle bulk sound velocity and density profiles can be obtained using any of the *a priori* models. However, the thermal structure associated with these compositional models differs significantly. Pyrolite yields a relatively cool geotherm ( $T_{660} \simeq 1800$  K and  $X_{\text{Pv}} \simeq 0.64$ ), while perovskite-rich models such as chondritic or cosmic models yield hot geotherms ( $T_{660} \simeq 2500$  K and  $X_{\text{Pv}} \simeq 0.84$  for the latter), but all of the geotherms are subadiabatic. The results of inversions are virtually unaffected by the partitioning of iron between perovskite and magnesiowustite. Out of the five oxide components considered in our models, the bulk Al<sub>2</sub>O<sub>3</sub> and CaO contents of the mineral assemblages are least well constrained from our inversions. Our results show that a major shortcoming of lower mantle compositional and thermal models based on inversions of bulk sound velocity and density is the strong dependence of the final solution on the *a priori* model. That is, a wide variety of best-fit compositional and thermal models can be obtained, all of which provide satisfactory fits to global average seismic models. It is, in fact, this non-uniqueness that dominates the resulting *a posteriori* uncertainties and prevents a clear discrimination between different compositional models. Independent constraints on the thermal structure or on the shear properties of lower mantle assemblages are needed to infer lower mantle composition with a higher degree of certainty.

**Key words:** bulk modulus, density, inverse problem, mantle, mineralogy, seismic velocities.

## 1 INTRODUCTION

The lower mantle accounts for nearly half of the mass of the Earth. It is generally accepted that its mineralogy mostly consists of magnesium silicate perovskite (Mg,Fe,Al)(Si,Al)O<sub>3</sub>, magnesiowustite

(Mg,Fe)O, and calcium silicate perovskite CaSiO<sub>3</sub> (e.g. Irifune 1994; Kesson *et al.* 1998). However, the exact proportions of these phases as well as the distribution of the elements between them (e.g. the partitioning of iron between perovskite and magnesiowustite) are not exactly known and the details of the chemical composition of the

lower mantle are still under debate. Whether or not the lower mantle has the same bulk composition as the upper mantle is fundamental for understanding global mantle dynamics, the thermal structure of the Earth and the nature and location of various geochemical reservoirs.

Since the 1960s, a large number of lower mantle compositions have been proposed. They range from essentially pure perovskite (Mg/Si  $\sim$  1) to compositions with a Mg/Si ratio as high as 1.3. The perovskite-rich class of models were introduced to keep the Mg/Si ratio for the bulk mantle close to that of chondrites; for example the CI chondrite hypothesis of Hart & Zindler (1986) and the EH chondrite model of Javoy (1995). These compositional models imply that the upper and lower mantle are chemically distinct. The second group of models corresponds to pyrolite-like composition. The original pyrolite model was proposed by Ringwood (1962a,b) and Green & Ringwood (1963) as a hypothetical mixture of olivine and pyroxene capable of producing the observed mid-oceanic basaltic magmas and a residual harzburgite upon partial melting. There now exist a large number of refined pyrolite models based on geochemical and petrological analysis, for example LOSIMAG1 (Hart & Zindler 1986), PRIMA (Allègre *et al.* 1995) and the pyrolite model of McDonough & Sun (1995). The hypothesis of an entire pyrolitic mantle implies that the mantle is depleted in silicon compared with chondrites. To explain a possible silicon depletion several scenarios have been proposed, invoking either siderophile behaviour of Si at moderate pressures or volatilization at high temperatures. Allègre *et al.* (1995) and McDonough & Sun (1995) put the missing silicon budget into the core whereas Ringwood (1979) suggested that Si was volatilized during Earth accretion.

In the past, a stratified mantle with independent reservoirs was proposed to explain geochemical observations such as the rare gas budget (e.g. Allègre *et al.* 1986). Such a model is, however, in contradiction with other geochemical observations, such as the ubiquitous signature of recycled material in all hotspots (Hofmann 1997) and with various geophysical observations: large-scale gravity field data (e.g. Richards & Hager 1984; Ricard *et al.* 1993) and modern seismic tomography. The latter indicates that some subducting slabs penetrate deep into the mantle (e.g. van der Hilst *et al.* 1997; Grand *et al.* 1997) suggesting some degree of mass exchange between the upper and lower mantle. Neither simple one-layer nor two-layer models of mantle convection can satisfy both the geophysical and the geochemical observations. More refined patterns of mantle convection have been proposed over the last decade (see e.g. Tackley 2000 for a review). Kellogg *et al.* (1999) argue that large mass transfer between the upper mantle and the lower mantle does not exclude inhomogeneous layers in the lowermost mantle. Coltice & Ricard (1999) and Ferrachat & Ricard (2001) show that one-layer mantle convection with partial oceanic crust segregation is not necessarily in contradiction with geochemical observations. Recent laboratory experiments carried out on two superimposed fluids suggest that the lower mantle may be in a convective transient state allowing a regime of oscillating domes, a stable stratified regime and a large-scale mixing regime (see Davaille *et al.* 2003 for a review). Consequently, the mode of convection is still questionable.

Most constraints on lower mantle composition and thermal structure come from comparing seismic velocities with experimentally measured properties of various mineral assemblages. The seismological parameters directly observable are the compressional wave velocities,  $V_p$ , and the shear wave velocities,  $V_s$ , and their lateral variations. However, the most abundant experimental results from mineral physics are the density  $\rho$ , and the isothermal bulk modulus,  $K_T$  (by static compression) or the adiabatic bulk modulus,  $K_S$  (by

acoustic methods). It is therefore more difficult to make use of shear properties as a constraint on mantle composition. For phases stable only at lower mantle conditions (e.g. silicate perovskite), results on  $V_p$  and  $V_s$  and shear properties are becoming available with the use of Brillouin spectroscopy (Sinogeikin *et al.* 2004; Jackson *et al.* 2004) and ultrasonic techniques (Aizawa *et al.* 2004; Sinelnikov *et al.* 1998) but such data are still comparatively few in number. A more commonly used approach is therefore to combine seismological models of  $V_p$  and  $V_s$  to generate bulk sound velocity  $V_\phi$  and density  $\rho$  models for comparison to mineralogical properties.  $V_\phi$  is related to the two seismic velocities via  $V_\phi^2 = V_p^2 - \frac{4}{3}V_s^2 = K_S/\rho$ , which leaves  $V_\phi$  independent of the shear modulus.

Seismological and mineralogical properties must of course be compared at similar conditions of pressure and temperature. This can be done either by adiabatic decompression of seismologically determined mantle properties for comparison at zero pressure with laboratory data (e.g. Bukowinski & Wolf 1990; Jackson 1998; Stacey & Isaak 2001) or by extrapolation of measured mineral properties to lower mantle  $P$ - $T$  conditions for comparison with seismologically determined bulk sound velocity and density profiles. Among the latter studies, some authors have proposed that a pyrolitic composition can reasonably match the seismological models without any iron or silicon enrichment (e.g. Fiquet *et al.* 2000; Jackson 1998; Wang & Weidner 1994; Wang *et al.* 1994). At the same time, other studies (e.g. Ita & Stixrude 1992) have disagreed with the idea of a uniform mantle and therefore favoured layered convection. Jeanloz & Knittle (1989), Bina & Silver (1997) and Stixrude *et al.* (1992) argued that the lower mantle should rather be chondritic or even pure perovskite. Several authors attempted to better constrain the lower mantle composition and its temperature by also including shear properties. Nevertheless, no clear consensus has emerged from these studies: Vacher *et al.* (1998) did not discriminate between homogeneous and stratified mantle models, Marton & Cohen (2002) preferred a pyrolitic lower mantle, and Wentzcovitch *et al.* (2004) suggested radially heterogeneous lower mantle models. In a recent study, Deschamps & Trampert (2004) showed that a radial density contrast in the mid-mantle could be obtained depending on the choice of elastic data together with a non-adiabatic geotherm.

Most of these studies only consider a three-component system (MgO-FeO-SiO<sub>2</sub>), neglecting the CaO and Al<sub>2</sub>O<sub>3</sub> content. However, all petrological models contain significant amounts of calcium and aluminium oxides (at least 5 wt%). The latter are essential in models of the upper mantle, since Al accounts for the presence of garnet and both Al and Ca strongly affect the phase relationships between the pyroxene-garnet components. In addition, aluminium oxide, even in small proportions, seems to drastically change the bulk properties of the magnesium silicate perovskite phase, as suggested by several studies (see Daniel *et al.* 2001; Andrault *et al.* 2001 for reviews). Contrary to aluminium, calcium does not enter the orthorhombic Mg-rich perovskite phase (e.g. Hirose *et al.* 1999) but instead is incorporated into a separate cubic CaSiO<sub>3</sub> perovskite phase. This phase has been often ignored due to its lesser abundance in the lower mantle (expected to be less than 5 mol%). It has been proposed that CaSiO<sub>3</sub> perovskite may be an invisible phase in terms of density and bulk modulus at lower mantle conditions (e.g. Shim *et al.* 2000), although Karki & Crain (1998) suggested that shear properties can allow the calcium budget of the lower mantle to be constrained. Because CaSiO<sub>3</sub> is almost certainly present in the lower mantle, we include it in our inversions to examine whether useful constraints can be placed on its abundance using the most recent measurements of physical properties.

All inversions of lower mantle composition are limited by a lack of information on the temperature profile. There is indeed a wide spectrum of proposed thermal structures. Brown & Shankland (1981) advocated a nearly adiabatic profile based on calculation of entropy. da Silva *et al.* (2000) deduced a strongly superadiabatic profile from mineral physics calculations (temperatures as high as 4000 K below 2500 km depth). These models are in contrast to numerical simulations of mantle convection mostly heated from within (Bunge *et al.* 2001; Monnereau & Yuen 2002) that suggest a subadiabatic lower mantle (as much as 400 K below an adiabat) except in a hot boundary layer above the core–mantle–boundary (CMB).

Given the uncertainties in elastic properties of minerals and thermal structure, the interpretation of 1-D seismic profiles is far from straightforward and is still controversial. In this study, we first select a set of recent and high-quality experimental data, then we apply a generalized inversion method to deduce the composition and temperature profile of the lower mantle. This method allows us to determine the composition and the temperature that best match global 1-D density and bulk sound velocity profiles reported by PREM (Dziewonski & Anderson 1981) and ak135 (Kennett *et al.* 1995). We also precisely evaluate which are the best constrained inverted parameters and examine the impact of experimental uncertainties on the resulting mineralogy and temperature. The shear properties are not considered for three reasons. First, bulk modulus and density are the most numerous and presumably best constrained parameters from experimental studies. Even though experimental measurements of mineral rigidities are becoming available, their pressure and temperature dependence is still poorly constrained. Indeed, for MgSiO<sub>3</sub> perovskite (the most abundant mineral in the lower mantle) only a few studies are available in a limited  $P$ – $T$  range (Sinelnikov *et al.* 1998; Sinogeikin *et al.* 2004). Second, the frequency dependence as well as the effect of viscoelastic relaxation on the shear properties of lower mantle minerals are still poorly known (Webb & Jackson 2003). Third, our results can be compared with previous studies that also used density and bulk sound velocity (or bulk modulus) as constraints for lower mantle properties. The formal inversion defined in this way allows us to study the effect

of Al and Ca as well as the possible non-uniqueness of the results, taking into account all available experimental elastic data and their uncertainties.

## 2 ELASTICITY DATA SET

The major features of the mineralogy of the lower mantle can be described by using three distinct phases: silicate perovskite (Mg,Fe,Al)(Si,Al)O<sub>3</sub> (Pv), magnesiowustite (Mg,Fe)O (Mw) and calcium-bearing perovskite CaSiO<sub>3</sub> (CaPv). The two perovskites are separate phases with limited solubility between them (e.g. Hirose *et al.* 1999). On the other hand, the solubility of aluminium in CaPv is not negligible (at most 10 mol%) as reported by Hirose *et al.* (1999) and Takafuji *et al.* (2002). These results come from experiments on MORB-like composition and grossular samples (all Al-rich compositions). In the case of pyrolite-like composition (magnesium-rich), aluminium enters the magnesium-rich perovskite and only a negligible amount of Al is found in CaPv (less than 2 mol%, Fei *et al.* 1996). Real wustite is in fact a non-stoichiometric compound, Fe<sub>1-x</sub>O. The stoichiometric extrapolation to  $x = 1$  used in this study leads to the purely fictitious end-member FeO (FeMw). It should be noted that the purpose of the fictive Fe end-members is to reproduce the elastic properties in the range of lower mantle iron content and they are not intended to obtain the actual properties of the pure iron end-members (FePv and FeMw).

In order to compute density and bulk sound velocity in the lower mantle (see Appendix A for details), we use a third-order Birch–Murnaghan equation of state (EoS). The following elastic properties of each end-member are required: molar volume at ambient conditions,  $V_0$ , isothermal bulk modulus,  $K_{0,T}$ , with its pressure and temperature derivatives,  $K'_{0,T}$  and  $(\partial K_{0,T}/\partial T)_P$ , respectively, and thermal expansion coefficient as a function of temperature,  $\alpha(T)$ . The elastic properties used in this study are listed in Table 1. In spite of significant progress in experimental techniques, not all of these properties are well constrained and a detailed discussion of their uncertainties is necessary. Our experimental data set is assembled through a careful review and selection of high-quality

**Table 1.** Elastic properties of lower mantle minerals: MgSiO<sub>3</sub> perovskite (MgPv), FeSiO<sub>3</sub> perovskite (FePv), Al<sub>2</sub>O<sub>3</sub> perovskite (AlPv) for the perovskite phase, MgO periclase (MgMw), FeO wustite (FeMw) for the magnesiowustite phase and CaSiO<sub>3</sub> perovskite (CaPv) for the calcium perovskite phase.

Mineral	$V_0$ (cm <sup>3</sup> mol <sup>-1</sup> )	$K_{0,T}$ (GPa)	$K'_{0,T}$	$(\partial K_{0,T}/\partial T)_P$ (GPa K <sup>-1</sup> )	$\alpha_0$ (10 <sup>-5</sup> K <sup>-1</sup> )	$\alpha_1$ (10 <sup>-8</sup> K <sup>-2</sup> )
MgPv	24.43 <sup>1</sup>	<b>250</b> <sup>2</sup> 246 <sup>5</sup> –261 <sup>6</sup>	4.0 <sup>3</sup>	-0.021 ± 0.004 <sup>4</sup>	2.461 ± 0.119	0.165 <sup>4</sup>
FePv	25.34 <sup>4</sup>	<b>250</b> <sup>b</sup> 246 <sup>5</sup> –261 <sup>6</sup>	4.0 <sup>b</sup>	-0.021 ± 0.004 <sup>b</sup>	2.461 ± 0.119	0.165 <sup>b</sup>
AlPv <sup>a</sup>	<b>24.58</b> <sup>7</sup> 24.51 <sup>4</sup>	<b>249</b> <sup>7</sup> 234 <sup>9</sup>	<b>4.0</b> <sup>8</sup> 4.0 <sup>9</sup>	<b>-0.021</b> <sup>b</sup> -0.06 <sup>9</sup>	<b>2.461</b> 2.12	<b>0.165</b> <sup>b</sup> 2.04 <sup>9</sup>
MgMw	11.25 <sup>10</sup>	<b>160.1</b> <sup>11</sup> 161.0 <sup>12</sup>	<b>3.83</b> <sup>11</sup> 3.94 <sup>12</sup>	-0.022 ± 0.001 <sup>4</sup> -0.022 <sup>12</sup>	<b>3.265</b> 3.000	<b>1.065</b> <sup>4</sup> 1.200 <sup>12</sup>
FeMw	12.26 <sup>4</sup>	160.1 <sup>4</sup>	3.83 <sup>4</sup>	-0.020 <sup>13</sup>	3.203	0.629 <sup>14</sup>
CaPv	27.45 <sup>15</sup> 27.45 <sup>16</sup>	232 <sup>15</sup> 236 <sup>16</sup>	4.8 <sup>15</sup> 3.9 <sup>16</sup>	-0.033 <sup>15</sup> -0.028 <sup>16</sup>	3.133 3.690	0.388 <sup>4</sup> 0.000 <sup>4</sup>

If multiple values are indicated, the preferred values are in bold.  $V_0$ , molar volume,  $K_{0,T}$ , isothermal bulk modulus,  $K'_{0,T}$  and  $(\partial K_{0,T}/\partial T)_P$ , its pressure and temperature derivatives;  $\alpha(T) = \alpha_0 + \alpha_1 T$ , thermal expansion coefficient.

<sup>a</sup>Al-bearing MgSiO<sub>3</sub> perovskite with 5 mol% Al<sub>2</sub>O<sub>3</sub>.

<sup>b</sup>Same as MgPv.

Sources: <sup>1</sup>e.g. Fiquet *et al.* (1998); <sup>2</sup>after Sinogeikin *et al.* (2004); <sup>3</sup>fixed to 4 as Fiquet *et al.* (1998); <sup>4</sup>see text; <sup>5</sup>Yeganeh-Haeri *et al.* (1989); <sup>6</sup>e.g. Mao *et al.* (1991); <sup>7</sup>after Jackson *et al.* (2004); <sup>8</sup>Daniel *et al.* (2004); <sup>9</sup>Zhang & Weidner (1999); <sup>10</sup>Jackson & Niesler (1982); <sup>11</sup>after Sinogeikin & Bass (2000); <sup>12</sup>Dewaele *et al.* (2000); <sup>13</sup>Sumino *et al.* (1980); <sup>14</sup>Skinner (1966); <sup>15</sup>Wang *et al.* (1996);

<sup>16</sup>Shim *et al.* (2000).

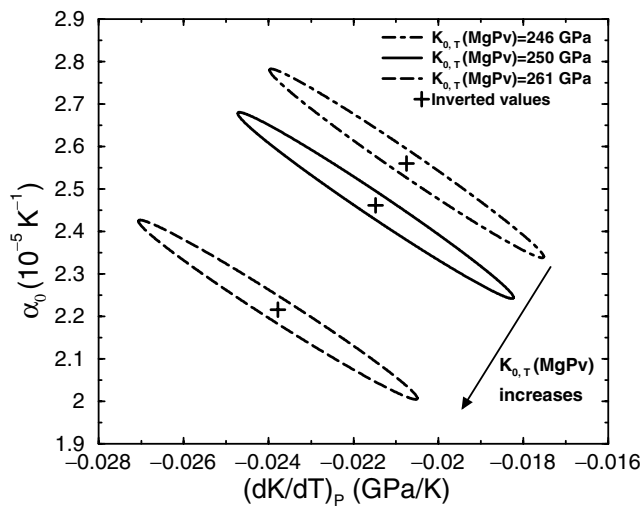


**Figure 1.** Values of  $(\partial K_{0,T}/\partial T)_P$  and  $\alpha_0$  for MgSiO<sub>3</sub> perovskite (MgPv) deduced from generalized inversions of  $P$ – $V$ – $T$  measurements assuming  $K_{0,T}$  (MgPv) is either equal to 246, 250 or 261 GPa. The  $P$ – $V$ – $T$  measurements are taken from Fiquet *et al.* (1998, 2000). The associated confidence ellipses ( $2\sigma$  level) indicate a strong anticorrelation between the two parameters. An increase in the nominal value of  $K_{0,T}$  shifts the confidence ellipse towards lower  $\alpha$  and  $(\partial K_{0,T}/\partial T)_P$  values (towards the lower left corner) revealing strong trade-offs between elastic parameters.

experimental data. Over the past years, the experimental techniques (static compression, ultrasonics, Brillouin techniques) have greatly matured and single-crystal properties have been found to be internally consistent. Moreover, recent experimental results using polycrystalline samples have in many cases come into agreement with single-crystal properties, with improvements in experimental methods. Where available, we adopt high-quality laboratory measurements of physical properties for our inversions, and use theoretical calculations of the necessary physical properties where experimental data are not available.

In this section, we review the elasticity database for the lower mantle minerals considered in our study. We see that for each parameter considered separately the experimental uncertainties are still very large, compared with the accuracy of the seismological models. These apparent discrepancies are, however, misleading. Due to the trade-off between elastic parameters inverted from experiments, very different parameter sets can reproduce very similar  $P$ – $V$ – $T$  measurements at mantle conditions. We illustrate this point in detail for the case of MgPv (see Fig. 1).

## 2.1 Molar volume $V_0$

This is the best constrained parameter. The most accurate and precise values of  $V_0$  come from conventional diffraction measurements made outside any high-pressure device at ambient conditions. These values are more accurate than those deduced from high  $P$ – $T$  experiments by simultaneously inverting experimental  $P$ – $V$ – $T$  data for  $V_0$  and other EoS parameters. For periclase,  $V_0$  can be directly measured at ambient conditions (Jackson & Niesler 1982). Due to the non-stoichiometry of wustite,  $V_0$  of pure fictive FeMw is obtained by extrapolation of experimental results on Fe<sub>1-x</sub>O, for  $x$  varying from 0.019 to 0.073 (Will *et al.* 1980; Hazen 1981; Yagi *et al.* 1985; Jeanloz & Sato-Sorensen 1986; Liu & Liu 1987). When  $V_0$  cannot be obtained independently and more accurately, such as for unquenchable CaSiO<sub>3</sub> perovskite, the value of  $V_0$  is deduced from

$P$ – $V$ – $T$  inversions of compression data (e.g. Wang *et al.* 1996; Shim *et al.* 2000). For MgSiO<sub>3</sub> perovskite the value of  $V_0$  is constrained by direct diffraction measurements at ambient conditions (e.g. Fiquet *et al.* 1998). The value of  $V_0$  for the pure virtual FePv end-member is determined by extrapolation of the measured volumes of perovskite samples with variable iron content, (Mg<sub>1-x</sub>,Fe<sub>x</sub>)SiO<sub>3</sub>: see Parise *et al.* (1990) ( $x = 0.1$ ), Mao *et al.* (1991) ( $x = 0.1, 0.2$ ), Wang *et al.* (1994) ( $x = 0.1$ ) and Andrault *et al.* (2001) ( $x = 0.05$ ). For  $V_0$  of AlPv, we use the value recently determined by Jackson *et al.* (2004) on aluminous MgSiO<sub>3</sub> perovskite (5 mol% Al<sub>2</sub>O<sub>3</sub>) by X-ray measurement. We also consider an alternative value deduced from extrapolation of volumes reported for perovskite samples with variable aluminium content,  $x$ Al<sub>2</sub>O<sub>3</sub> + (1 –  $x$ ) MgSiO<sub>3</sub>: see Zhang & Weidner (1999) ( $x = 0.05$ ), Andrault *et al.* (2001) ( $x = 0.11$ ), Daniel *et al.* (2001) ( $x = 0.077$ ), Daniel *et al.* (2004) ( $x = 0.05$ ), Jackson *et al.* (2004) ( $x = 0.05$ ) and Yagi *et al.* (2004) ( $x = 0.012, 0.103$ ).

## 2.2 Bulk modulus $K_{0,T}$ and its pressure derivative $K'_{0,T}$

The volume (and density) at standard conditions is generally not controversial. However, with the bulk modulus and its pressure and temperature derivatives there are sometimes significant discrepancies between values when multiple measurements are available. Therefore, we had to prioritize the data from various sources. Where available, the results from ultrasonic techniques and Brillouin spectroscopy performed on single crystals are preferred over data from static compression or acoustic measurements on polycrystalline specimens. In many cases, the two approaches give quite similar results (e.g. for MgPv Sinogeikin *et al.* (2004) give  $K_{0,S} = 253(9)$  GPa whereas Fiquet *et al.* (2000) give  $K_{0,T} = 253(3)$  GPa). In cases where there are substantial differences (for example AlPv EoS data) we use diffraction results as an alternative set of parameters.

The compressibility of periclase MgO has been widely studied and is well constrained by Brillouin scattering (Sinogeikin & Bass 2000) and ultrasonic (e.g. Jackson & Niesler 1982) measurements. Compatible results are obtained from X-ray diffraction measurements in a diamond anvil cell (e.g. Dewaele *et al.* 2000). The values for FeO are obtained from measurements on a non-stoichiometric wustite, e.g. Fe<sub>0.943</sub>O (Jackson *et al.* 1990), or from extrapolation of measurements on MgO–FeO (Fei 1999; Kung *et al.* 2002). These studies suggest that  $K_{0,T}$  of wustite is lower than that of periclase. However, a recent study by Jacobsen *et al.* (2002) shows that the bulk modulus of (Mg<sub>1-x</sub>,Fe<sub>x</sub>)O remains relatively constant (within experimental uncertainties) up to at least  $x = 0.3$ . Therefore, to simulate lower mantle magnesiowustite properly (i.e. with  $x < 0.3$ ), we choose a bulk modulus of FeMw equal to the bulk modulus of MgMw. Two recent studies on CaSiO<sub>3</sub> perovskite based on X-ray diffraction measurements (Wang *et al.* 1996; Shim *et al.* 2000) give similar incompressibilities even though they propose numerically different sets of  $K_{0,T}$  and  $K'_{0,T}$  (see Table 1). The two sets of values describe equally well very similar  $P$ – $V$ – $T$  measurements and the apparent differences are only due to strong trade-offs between inverted elastic parameters.

Although (Mg,Fe,Al)-bearing perovskite is the most abundant phase in the lower mantle, there is not a complete consensus on its incompressibility. The reported experimental values of  $K_{0,T}$  for pure MgSiO<sub>3</sub> perovskite range from 246 to 261 GPa (e.g. Yeganeh-Haeri *et al.* (1989) and Sinogeikin *et al.* (2004) both using Brillouin scattering, and Mao *et al.* (1991), Wang *et al.* (1994), Utsumi *et al.* (1995), Funamori *et al.* (1996), Fiquet *et al.* (1998, 2000), Saxena

*et al.* (1999) and Andrault *et al.* (2001) using the X-ray diffraction technique). A value of  $K_{0,S} = 253(5)$  GPa, which corresponds to  $K_{0,T} \simeq 250(5)$  GPa taking into account the appropriate correction (see Appendix A), has recently been measured by Brillouin spectroscopy (Sinogeikin *et al.* 2004), agreeing within the error-bars with  $K_{0,T} = 253(9)$  GPa obtained from previous  $P$ - $V$ - $T$  data by Fiquet *et al.* (2000). As for  $K'_{0,T}$ , its value is often fixed more or less arbitrarily to 4. A better resolution of  $K'_{0,T}$  would require a larger number of precise simultaneous high- $P$  and high- $T$  measurements to reduce the strong correlations between  $V_0$ ,  $K_{0,T}$  and  $K'_{0,T}$ . Fiquet *et al.* (2000) considered all available  $P$ - $V$ - $T$  measurements to perform a generalized inversion and obtained  $K'_{0,T} = 3.7$  together with  $K_{0,T} = 260$  GPa. Given the uncertainties on  $K_{0,T}$ ,  $(\partial K_{0,T}/\partial T)_P$  (see discussion below) and intrinsic correlations, we keep  $K'_{0,T}$  equal to 4. The effect of iron on the bulk modulus of perovskite has not been clearly identified yet. Several studies suggest that small amounts of iron (less than 10 mol%) have only a negligible effect on  $K_{0,T}$  and  $K'_{0,T}$  of iron-bearing perovskite, within the experimental error bars (Mao *et al.* 1991; Knittle & Jeanloz 1987). However, there are some indications that iron could make perovskite somewhat stiffer, but there is no agreement on the magnitude of this phenomenon. Andrault *et al.* (2001) reported that 5 mol% of iron increases the bulk modulus by 2.7 per cent whereas Kiefer *et al.* (2002) calculated using a first-principles method that 25 mol% of iron increases  $K_{0,T}$  by only 1.9 per cent.

As for aluminium, both theoretical (Brodholt 2000; Yamamoto *et al.* 2003) and experimental studies (Zhang & Weidner 1999; Daniel *et al.* 2001, 2004; Jackson *et al.* 2004; Yagi *et al.* 2004) have shown that the dissolution of  $\sim 5$  mol% of  $\text{Al}_2\text{O}_3$  into the perovskite structure decreases its bulk modulus. There is, however, no agreement on the amplitude and physical basis for this phenomenon: some experimental results on Al-bearing perovskite (5 mol%  $\text{Al}_2\text{O}_3$ ) show a decrease of 0–1 per cent (Daniel *et al.* 2004; Jackson *et al.* 2004) whereas others show a decrease of 7 per cent (Zhang & Weidner 1999) compared with the bulk modulus of pure  $\text{MgSiO}_3$  perovskite. It should also be noticed that Andrault *et al.* (2001) reported contrasting behaviour suggesting a stiffer Al-bearing perovskite structure. In this study, we choose the most recent Brillouin results on Al-bearing perovskite (with 5 mol% of  $\text{Al}_2\text{O}_3$ ) by Jackson *et al.* (2004). We also assume, as in the case of iron, that aluminium has no significant effect on  $K'_{0,T}$ , as supported by recent experiments by Daniel *et al.* (2004).

### 2.3 $(\partial K_{0,T}/\partial T)_P$ and thermal expansion $\alpha$

These parameters are often obtained by inversion of  $P$ - $V$ - $T$  measurements. As a result, they are highly correlated.  $(\partial K_{0,T}/\partial T)_P$  is considered to be constant as a function of temperature. Thermal expansion is usually given as a non-linear function with empirically determined coefficients. It can be shown that within the actual experimental uncertainties, a linear increase of  $\alpha$  with temperature is sufficient to fit experimental observations.

The values reported from separate  $P$ - $V$ - $T$  studies can differ significantly even though they have been obtained by matching similar observed densities. In order to assess the effect of uncertainties on these correlated parameters in a self-consistent way, we need to know the associated covariance matrix. However, the latter is not usually reported. We revisited the data from Fiquet *et al.* (1998) and Fiquet *et al.* (2000) to compute  $(\partial K_{0,T}/\partial T)_P$  and  $\alpha$  of MgPv using a generalized inverse method (Tarantola & Valette 1982). In addition to the inverted parameters and their uncertainties (which we found in agreement with Fiquet *et al.* 2000), we also computed the complete

associated covariance matrix. We notice that the inverted value of  $-0.021$  GPa  $\text{K}^{-1}$  for  $(\partial K_{0,T}/\partial T)_P$  is in agreement with several other studies (Wang *et al.* 1994; Utsumi *et al.* 1995; Funamori *et al.* 1996; Fiquet *et al.* 1998, 2000; Gillet *et al.* 2000).

For MgPv, Fig. 1 depicts the resulting confidence ellipses within the  $2\sigma$  range in the simultaneous determination of  $\alpha$  and  $(\partial K_{0,T}/\partial T)_P$ , with fixed  $V_0$ ,  $K_{0,T}$  and  $K'_{0,T}$ . Similar correlations between EoS parameters have been already discussed by Bass *et al.* (1981) and Angel (2001) using the same Birch–Murnaghan formulation, and by Jackson *et al.* (1990) using Mie–Grüneisen–Debye parametrization. In this study, we perform three inversions by fixing  $K_{0,T}$  to 246 GPa (Yeganeh-Haeri *et al.* 1989), 250 GPa (preferred value, Sinogeikin *et al.* 2004) or 261 GPa (e.g. Mao *et al.* 1991).  $V_0$  and  $K'_{0,T}$  are fixed to previously discussed values. Whatever the chosen value of  $K_{0,T}$ , the final inverted set of parameters gives a good fit to the  $P$ - $V$ - $T$  data set. Fig. 1 also shows that increasing the nominal value of  $K_{0,T}$  shifts the inverted  $\alpha$  and  $(\partial K_{0,T}/\partial T)_P$  towards lower values. It clearly reveals strong anticorrelations between the inverted elastic parameters. These three parameter sets will be used to study the influence of uncertainties on elastic parameters of MgPv by random sampling of  $(\partial K_{0,T}/\partial T)_P$  and  $\alpha$  within these  $2\sigma$  ellipses.

The effect of aluminium on the thermal equation of state of perovskite has been studied by Zhang & Weidner (1999) who reported a value of  $(\partial K_{0,T}/\partial T)_P$  close to  $-0.06$  GPa  $\text{K}^{-1}$ . This value is significantly higher than reported values for any other mantle minerals, and in particular it is above the experimental values for MgPv. Due to the intrinsic trade-offs, this value cannot be considered alone because it was obtained together with a significantly low value of  $K_{0,T}$  (234 GPa) and an unusually high value of  $\alpha$  ( $\sim 6 \times 10^{-5}$   $\text{K}^{-1}$  at 2000 K). We note that high (negative) values of  $(\partial K_{0,T}/\partial T)_P$  were also reported by Mao *et al.* (1991) and Stixrude *et al.* (1992) for  $\text{MgSiO}_3$  perovskite. Wang *et al.* (1994) suggested that these high values are probably due to partial back-transformation, or even to partial amorphization. We choose this parameter set as an alternative one. In the case of iron-bearing perovskite, there is no evidence for a change of either  $(\partial K_{0,T}/\partial T)_P$  or thermal expansivity due to dissolution of iron into the perovskite structure (Hama & Suito 1998; Anderson & Hama 1999). Therefore, we choose the same values for FePv as for MgPv.

In the case of  $\text{CaSiO}_3$  perovskite, the available  $(\partial K_{0,T}/\partial T)_P$  comes from two previously mentioned studies (Wang *et al.* 1996; Shim *et al.* 2000) but the thermal expansion is not well constrained. Wang *et al.* (1996) obtained the best fit to their measurements by assuming a constant thermal expansion coefficient equal to  $3 \times 10^{-5}$   $\text{K}^{-1}$ . Extrapolation of this value using the Birch–Murnaghan EoS leads to a negative thermal expansion at high pressure (above  $\sim 75$  GPa) and high temperature (above  $\sim 2200$  K) for CaPv. Therefore, we re-evaluate the thermal expansion of these two studies using the same inversion of  $P$ - $V$ - $T$  measurements as previously described for MgPv. We set  $V_0$ ,  $K_{0,T}$  and  $(\partial K_{0,T}/\partial T)_P$  to the respective values of Wang *et al.* (1996) and Shim *et al.* (2000) and invert for thermal expansion coefficients,  $\alpha_0$  and  $\alpha_1$ . The data of Shim *et al.* (2000) do not allow us to constrain  $\alpha_1$ . The best fit is then obtained when  $\alpha_1 = 0$ . The inversion of the two data sets leads to thermal expansions of the order of  $3.7 \times 10^{-5}$   $\text{K}^{-1}$  at lower mantle temperatures. This value is slightly higher than the fixed value of  $3 \times 10^{-5}$   $\text{K}^{-1}$  reported by Wang *et al.* (1996), and displays reasonable behaviour at lower mantle  $P$ - $T$  conditions (see Table 1).

For periclase, we average the thermal expansion obtained by Suzuki (1975) from dilatometric measurements and by Fiquet *et al.*

(1999) from X-ray diffraction measurements.  $(\partial K_{0,T}/\partial T)_P$  is inverted from  $P$ – $V$ – $T$  measurements of Dewaele *et al.* (2000), fixing the values of  $V_0$ ,  $K_{0,T}$ ,  $K'_{0,T}$  and  $\alpha$ . It is in agreement with previous values reported by Isaak *et al.* (1989, 1990), Utsumi *et al.* (1998), Fei (1999), Zhang (2000) and Sinogeikin *et al.* (2000). We notice that the resulting uncertainty is small. This is not surprising since  $(\partial K_{0,T}/\partial T)_P$  is the only free parameter. To take into account experimental uncertainties, we choose the parameters given by Dewaele *et al.* (2000) as an alternative set. Finally, there is a little information on the behaviour of MgO–FeO solid solutions at high temperature, leaving  $(\partial K_{0,T}/\partial T)_P$  and  $\alpha$  of these compositions poorly constrained. In this study, we use the value of  $(\partial K_{0,T}/\partial T)_P$  of wustite given by Sumino *et al.* (1980) who conducted experiments to determine the adiabatic bulk modulus on non-stoichiometric wustite  $\text{Fe}_{0.92}\text{O}$ . The value of  $\alpha$  of FeMw has been measured by X-ray diffraction measurements by Skinner (1966).

### 3 INVERSION TECHNIQUE

The density and bulk sound velocity profiles in the lower mantle reflect its mineralogical composition as well as its thermal structure. We can therefore formulate an inverse problem in order to extract these characteristics from seismological observations. In this study, we use the generalized inverse method proposed by Tarantola & Valette (1982).

The observations (the data vector  $\mathbf{d}_0$ ) consist of values of density and bulk sound velocity. They are deduced from PREM (Dziewonski & Anderson 1981) and ak135 (Kennett *et al.* 1995) at various depths. The molar abundances of each end-member and the temperature at these depths are the model parameters (the vector  $\mathbf{p}$ ). The forward problem, mathematically expressed as  $\mathbf{d} = g(\mathbf{p})$ , relates any set of model parameters to a data vector  $\mathbf{d}$ , which is generally different from  $\mathbf{d}_0$ . The operator  $g$  reflects the procedure of computing density and bulk sound velocity for a given mantle composition, pressure and temperature.  $g$  cannot be expressed as a simple expression and we use a numerical code to compute the forward problem.

The inverse problem is to derive a parameter set  $\hat{\mathbf{p}}$  that explains the observations within their uncertainties and remains reasonably close (depending on our knowledge) to an *a priori* guess  $\mathbf{p}_0$ . In other words, we are looking for  $\mathbf{p}$  that minimizes the following misfit function:

$$\mathbf{S}(\mathbf{p}) = [\mathbf{d}_0 - g(\mathbf{p})]^T \mathbf{C}_{\mathbf{d}_0\mathbf{d}_0}^{-1} [\mathbf{d}_0 - g(\mathbf{p})] + (\mathbf{p} - \mathbf{p}_0)^T \mathbf{C}_{\mathbf{p}_0\mathbf{p}_0}^{-1} (\mathbf{p} - \mathbf{p}_0) \quad (1)$$

where  $\mathbf{C}_{\mathbf{d}_0\mathbf{d}_0}$  and  $\mathbf{C}_{\mathbf{p}_0\mathbf{p}_0}$  are covariance matrices corresponding to our *a priori* confidence in the data and *a priori* knowledge of model parameters. In this study, we assume that data and parameters are uncorrelated. Therefore, the covariance matrices are diagonal and contain the squares of uncertainties on observations,  $\mathbf{C}_{\mathbf{d}_0\mathbf{d}_0}$ , and on parameters,  $\mathbf{C}_{\mathbf{p}_0\mathbf{p}_0}$ . We adopt the reported uncertainties on density and bulk sound velocity of 0.5 per cent (Silver *et al.* 1988) and 0.1 per cent (Kennett *et al.* 1995), respectively. Our *a priori* model  $\mathbf{p}_0$  corresponds to a pyrolite-like composition, which is often assumed to be an average lower mantle composition (e.g. Ringwood 1982), and the temperature profile proposed by Brown & Shankland (1981). The latter is a reasonable approximation of a mantle adiabat. However, it should be noted that there is no physical reason why the actual geotherm should correspond to an isentrope. The uncertainty on each molar abundance is arbitrarily set to 50 per cent and to  $\sim 400$  K for temperature.

The minimization is performed iteratively using standard procedures (for details see Tarantola & Valette 1982). Besides the best-

fitting model  $\hat{\mathbf{p}}$ , this method allows us to evaluate the associated *a posteriori* uncertainties and covariance matrix. We choose the starting model to coincide with the *a priori* model.

## 4 RESULTS

In this section, we perform several numerical experiments to test a series of possible sets of elastic constants and of partitioning coefficients. We also study the effect of various *a priori* models on global chemical composition and thermal structure. In all cases, the inverted parameter sets match seismic observations within their stated uncertainties (as discussed above).

The best-fitting model of lower mantle composition and temperature depends on our confidence in the *a priori* parameters (i.e. values of  $\mathbf{C}_{\mathbf{p}_0\mathbf{p}_0}$ ), in the seismological data (i.e. values of  $\mathbf{C}_{\mathbf{d}_0\mathbf{d}_0}$ ) and also in the physical modelling of  $g$  (i.e. modelling errors, Tarantola 1987). Modelling uncertainties come from the non-uniqueness in estimating averaged properties (e.g. Stacey 1998), from the inaccuracies of the elastic constants and from imprecisely constrained models of the iron partitioning between perovskite and magnesiowustite. While the effect of the parameter and data uncertainties is automatically expressed by the *a posteriori* covariance matrix, the influence of the model uncertainty is not straightforward to evaluate. Our approach will be to randomly test a series of possible sets of elastic constants and partitioning coefficients.

To represent the inverted composition of the lower mantle, we use the common representation in terms of molar fraction of magnesium-rich silicate perovskite,  $X_{\text{Pv}}$ , and calcium silicate perovskite,  $X_{\text{Ca}}$  defined as follows:

$$X_{\text{Pv}} = \frac{\text{Pv}}{\text{Pv} + \text{Mw} + \text{CaPv}} \\ X_{\text{Ca}} = \frac{\text{CaPv}}{\text{Pv} + \text{Mw} + \text{CaPv}} \quad (2)$$

where Pv, Mw and CaPv are the molar abundances of perovskite, magnesiowustite and calcium-perovskite phases. The molar fraction of magnesiowustite is then simply given by:

$$X_{\text{Mw}} = 1 - X_{\text{Pv}} - X_{\text{Ca}}. \quad (3)$$

The iron content of the mantle is characterized by the molar ratio

$$X_{\text{Fe}} = \frac{\text{Fe}}{\text{Fe} + \text{Mg}} \quad (4)$$

where Fe and Mg indicate the bulk molar abundances. For the *a priori* pyrolite composition,  $X_{\text{Pv}} = 0.622$ ,  $X_{\text{Mw}} = 0.327$ ,  $X_{\text{Ca}} = 0.051$  and  $X_{\text{Fe}} = 0.104$ .

We perform calculations from 800 to 2700 km depth to avoid effects due to either phase changes associated with the 660 km discontinuity and/or a possible thermal and compositional boundary layer at the base of the mantle. The transition from garnet to perovskite is likely to extend far below 660 km (e.g. Hirose *et al.* 1999; Irifune *et al.* 1996) enhanced by the presence of Al-rich subducting slabs. At the bottom of the mantle, the radial seismic profiles are perturbed due to the topography and the complex nature of  $D''$  (e.g. Lay *et al.* 1998). These effects may significantly change the slopes of the radial seismic profiles.

### 4.1 Influence of iron partitioning

The partitioning of iron between perovskite and magnesiowustite relates molar abundances of four among six end-member abundances in the lower mantle (MgPv, FePv, MgMw, FeMw). The corresponding partition coefficient  $K_D$  is usually defined by:

**Table 2a.** Enthalpy of formation  $\Delta H_0^f$ , and entropy  $S_0$ , at standard conditions,  $P_0 = 1$  bar and  $T_0 = 298$  K.

	$\Delta H_0^f$ (kJ mol <sup>-1</sup> )	$S_0$ (J mol <sup>-1</sup> K <sup>-1</sup> )
MgPv	-1442.50 <sup>1</sup>	58.29 <sup>2</sup>
FePv	-1090.10 <sup>1</sup>	100.77 <sup>1</sup>
MgMw	-601.49 <sup>1</sup>	26.94 <sup>1</sup>
FeMw	-267.27 <sup>1</sup>	57.59 <sup>1</sup>

Sources: <sup>1</sup> Fei *et al.* (1991); <sup>2</sup> vibrational approach after Gillet *et al.* (2000).

$$K_D = \frac{X_{\text{Fe}}^{\text{Pv}} / X_{\text{Mg}}^{\text{Pv}}}{X_{\text{Fe}}^{\text{Mw}} / X_{\text{Mg}}^{\text{Mw}}}. \quad (5)$$

It has been reported that in Al<sub>2</sub>O<sub>3</sub>-free systems, Fe preferentially partitions into magnesiowustite rather than into perovskite giving values of  $K_D$  around 0.25 (Katsura & Ito 1996; Mao *et al.* 1997; Martinez *et al.* 1997; Frost & Langenhorst 2002). The influence of pressure, temperature and bulk iron content on  $K_D$  is, however, not clearly quantified (e.g. Mao *et al.* 1997). It has also been shown that the iron partitioning is strongly coupled to the Al<sub>2</sub>O<sub>3</sub> content, but this effect remains poorly constrained. Wood & Rubie (1996) reported a  $K_D$  value of 1 at 25 GPa and 1873 K in a peridotitic sample containing 4 to 5 wt% of Al<sub>2</sub>O<sub>3</sub> whereas Andraut (2001) proposed a  $K_D$  at 2200 K ranging from 0.8 at 51 GPa to 3.2 at 94 GPa for the same Al<sub>2</sub>O<sub>3</sub> content added to an olivine composition sample.

To cover this large experimental range, we choose two characteristic values of  $K_D$ :  $K_D^{(1)} = 1.0$  and  $K_D^{(2)} = 0.25$ . We also consider the value of partition coefficient,  $K_D^{(3)}$ , obtained assuming thermodynamic equilibrium. In that case, we solve the following equation:

$$\mu_{\text{MgPv}}(P, T) + \mu_{\text{FeMw}}(P, T) = \mu_{\text{FePv}}(P, T) + \mu_{\text{MgMw}}(P, T) \quad (6)$$

where the  $\mu_i$  are the chemical potentials at pressure  $P$  and temperature  $T$  of each end-member  $i$ , MgPv, FePv, MgMw and FeMw. Each chemical potential  $\mu_i$  is given by:

$$\mu_i(P, T) = \mu_i^0(P, T) + RT \ln a_i(P, T, n_i) \quad (7)$$

where  $n_i$  is the molar abundance of the end-member  $i$ . The standard chemical potentials  $\mu_i^0$  are computed using thermodynamic data summarized in Tables 1, 2a and 2b. The activity–composition relationships  $a_i$  are poorly constrained for lower mantle assemblages. The non-ideality of solid solutions is usually expressed in terms of empirical Margules parameters  $W$ .  $W$ , however, depends on the particular choice of standard chemical potentials and reference mixing models (e.g. Fei *et al.* 1991). We cannot use at the same time standard

chemical potentials and Margules parameters taken from two different studies. In this paper, we thus assume an ideal on-site mixing model (Spear 1995) for perovskite and magnesiowustite phases. The computed equilibrium partition coefficient  $K_D^{(3)}$  is almost constant at around 0.8 throughout the lower mantle.

The three inversions with the three different partitioning coefficients lead to uniform compositions throughout the lower mantle (see Fig. 2). The inverted bulk composition is rather similar to the pyrolite composition (see Table 3). For  $K_D = 1$ , the resulting  $X_{\text{Pv}} = 0.643$  is higher by 3 per cent and  $X_{\text{Ca}} = 0.054$  by 7 per cent whereas  $X_{\text{Fe}} = 0.096$  is lowered by 7 per cent compared with the *a priori* pyrolite composition. The temperature profile is subadiabatic and colder by 180 K in the mid-mantle compared with the geotherm of Brown & Shankland (1981). The results obtained with  $K_D^{(1)}$  and  $K_D^{(3)}$  are indistinguishable. In the case of  $K_D^{(2)}$ , the inverted geotherm is closer to the *a priori* estimation than in the other two cases, but the composition remains very similar. The insensitivity of the inversion to the iron partitioning has already been discussed by Jackson (1998), Stacey & Isaak (2001) and Marton & Cohen (2002).

These global results are a little different from previously published conclusions. For example, Jackson (1998) proposed a pyrolite-like composition with  $X_{\text{Pv}} = 0.67$  and  $X_{\text{Fe}} = 0.11$ . A direct comparison with his results is not straightforward since he limited the inversion to a three-component system MgO–FeO–SiO<sub>2</sub>. When our values are transformed from a five- to a three-component system by putting  $\text{CaPv} = \text{AlPv} = 0$  in eq. (2), we obtain  $X_{\text{Pv}} = 0.73$  and  $X_{\text{Fe}} = 0.10$ . We think that these differences may be due mainly to a different choice of elastic parameters. Jackson (1998) used higher  $K_{0,T}$  for perovskite and for magnesiowustite. He chose  $K_{0,S} = 264$  GPa for perovskite instead of 253 GPa in this study and  $K_{0,S} = 162.5$  GPa with  $K'_{0,S} = 4.13$  for magnesiowustite instead of 161 GPa and 3.83, respectively, in this study (see further discussion in Section 4.5).

As for the temperature, we obtain a value at the 660 km discontinuity  $T_{660}$  of  $\sim 1800$  K which is very close to the  $T_{660} \simeq 1900 \pm 100$  K obtained from experimental study by Ito & Katsura (1989). The temperature at the core–mantle boundary  $T_{\text{CMB}}$  is close to 2250 K. These results are also in agreement with  $T_{660} \simeq 1850$  K and  $T_{\text{CMB}} \simeq 2300$  K proposed by Jackson (1998).

Fig. 2 also suggests some anomalous behaviour of the iron content from 660 km down to about 1300 km depth. One can observe a progressive transition from an iron-enriched top of the lower mantle to a mid-mantle (from 1000 km and deeper) having the same iron content as pyrolite. This behaviour is correlated with a strongly subadiabatic temperature gradient (the geotherm is basically flat down to 1000 km). These features may be indicating one or more

**Table 2b.** Heat capacities at standard pressure  $P = 1$  bar.

	$C_p^a$ (J mol <sup>-1</sup> K <sup>-1</sup> )						
	$a_1$ (10 <sup>2</sup> )	$a_2$ (10 <sup>-2</sup> )	$a_3$ (10 <sup>7</sup> )	$a_4$ (10 <sup>-6</sup> )	$a_5$ (10 <sup>9</sup> )	$a_6$ (10 <sup>4</sup> )	$a_7$ (10 <sup>4</sup> )
MgPv	0.361 <sup>b</sup>	1.576	0.415	0.870	-0.072	0.476	-8.284
FePv	1.422 <sup>c</sup>	0.154	-0.119	0.000	0.274	0.000	-1.454
AlPv	1.166 <sup>d</sup>	0.155	-0.590	1.624	0.676	0.043	-0.607
MgMw	0.334 <sup>b</sup>	0.430	0.006	0.402	0.040	0.092	-1.596
FeMw	0.684 <sup>c</sup>	0.119	0.170	0.000	0.135	0.000	-1.188
CaPv	0.970 <sup>d</sup>	0.811	-0.221	1.845	0.355	0.167	-3.100

$$^a C_p(T) = a_1 + a_2 T + a_3 T^{-2} + a_4 T^2 + a_5 T^{-3} + a_6 T^{-1/2} + a_7 T^{-1}.$$

<sup>b</sup>Vibrational approach after Gillet *et al.* (2000).

<sup>c</sup>From Fei *et al.* (1991).

<sup>d</sup>Debye model.

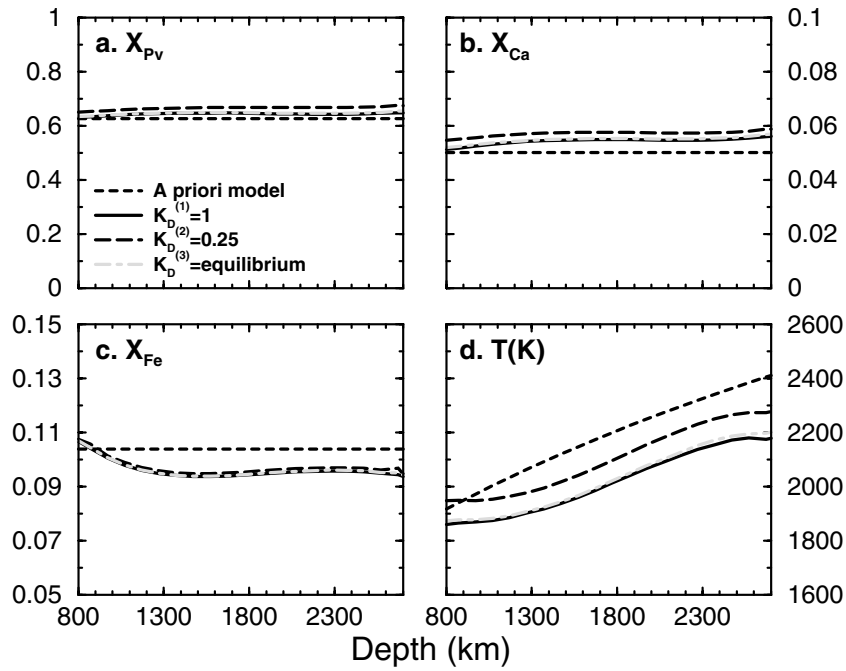


**Figure 2.** Influence of iron partitioning on lower mantle composition (a, b, c) and temperature (d). The dashed curves represent the *a priori* model: the pyrolite composition and the geotherm given by Brown & Shankland (1981). Other curves correspond to different values of the partitioning coefficient  $K_D^{(1)} = 1$  (solid),  $K_D^{(2)} = 0.25$  (long dashed),  $K_D^{(3)}$  computed from thermodynamic equilibrium (light dot-dashed). The predicted geotherms are subadiabatic and cooler than the *a priori* temperature profile by  $\sim 180$  K in the mid-mantle.

**Table 3.** Average inverted compositions assuming different iron partitioning  $K_D$  and compared with *a priori* pyrolite composition (Ringwood 1982). See eqs (2) and (4) for definitions of  $X_{Pv}$ ,  $X_{Ca}$  and  $X_{Fe}$ .

	$X_{Pv}$	$X_{Ca}$	$X_{Fe}$
Pyrolite	0.622	0.051	0.104
$K_D^{(1)} = 1$	$0.643 \pm 0.172$	$0.054 \pm 0.036$	$0.096 \pm 0.062$
$K_D^{(2)} = 0.25$	$0.664 \pm 0.159$	$0.057 \pm 0.038$	$0.097 \pm 0.050$

phase changes in the vicinity of 660 km or at greater depth that are smeared by the seismic profiles. Indeed, one can observe a larger velocity gradient in both PREM and ak135 models to about 1300 km depth, which may be related to the anomalous behaviour of iron content and the subadiabatic temperature profile in this region. We also notice that the anomalous behaviour of iron is not observed at the base of the mantle. A mild flattening of the geotherm appears again from 2600 km depth. In general, the inverted temperature profiles present a sigmoidal shape, i.e. they are not as smooth as simple adiabats (e.g. Jackson 1998). This possibly reflects phase changes and/or changes of bulk composition with depth.

In the following sections, we fix  $K_D = 1$ . This model with the *a priori* pyrolite composition and the geotherm of Brown & Shankland (1981) is denoted the M1 model, and its associated inverted model, IM1 (‘inverted model 1’).

## 4.2 Resulting *a posteriori* uncertainties

The results discussed above should be considered carefully in the light of *a posteriori* uncertainties. We have set large *a priori* uncertainties on parameters in order to investigate a large parameter space. These uncertainties do not necessarily have a precise physical meaning (one can easily choose uncertainties of 800 K instead

of 400 K for temperature and of 25 per cent instead of 50 per cent for composition). What is indeed relevant to consider here is how the *a posteriori* uncertainties on each parameter decrease relative to the *a priori* ones. The more the *a posteriori* uncertainties are lowered, the more certainty we have of the inverted parameters. It is in this way that we evaluate whether a parameter is well resolved or not. In Fig. 3, we compare the *a priori* and *a posteriori* uncertainties assuming an iron partitioning equal to 1. We can see that the inversion does not allow us to equally constrain all parameters.  $X_{Pv}$ ,  $X_{Fe}$  and the temperature profile are better constrained than  $X_{Ca}$  since their *a posteriori* uncertainties are significantly smaller than their *a priori* values (see Fig. 3). The same *a posteriori* error bars are shown in Fig. 4 in terms of uncertainties on the six end-members. These two figures reveal that the resolution of all parameters is constant with depth and that density and bulk sound velocity do not put significant constraints on either the calcium or the aluminium content of the lower mantle. Moreover, one can read in Table 3 that even though the inversion gives results close to pyrolite composition, other possible compositions for the lower mantle such as a silicon-enriched model are acceptable due to the large error bars.

Our approach also makes it possible to compute an appropriate *a posteriori* covariance matrix which provides information on correlations and trade-offs between inverted parameters. Fig. 5 depicts the covariance matrix in the mid-mantle (this covariance matrix is mostly depth independent). Since the global formula for the lower mantle assumes 1 mol of MgPv and since FePv is given by the partition coefficient  $K_D$ , only five independent parameters are plotted in this matrix (molar abundances of MgMw, FeMw, CaPv, AlPv and temperature  $T$ ). This shows that MgMw is strongly correlated to FeMw, whereas the temperature is anticorrelated to both MgMw and FeMw. CaPv and AlPv are not significantly correlated with any other parameters.

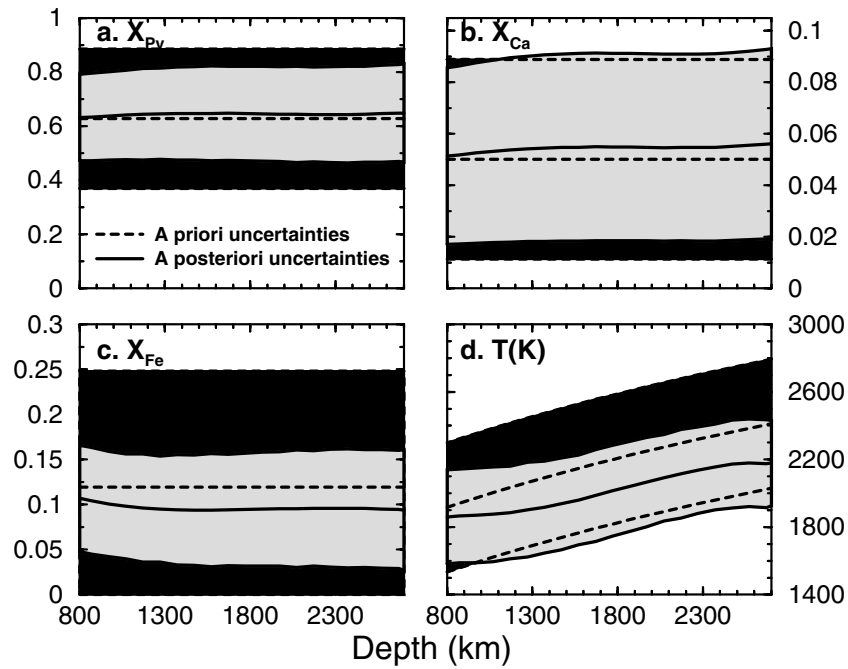


**Figure 3.** Inverted depth-dependent profiles of  $X_{Pv}$ ,  $X_{Ca}$ ,  $X_{Fe}$  and temperature  $T$  with their *a priori* and *a posteriori* uncertainties (light and dark grey shading). The *a priori* model is pyrolite composition and the geotherm of Brown & Shankland (1981).  $X_{Fe}$  and temperature are rather well resolved.  $X_{Ca}$  is not constrained by inversion of density and bulk sound velocity.

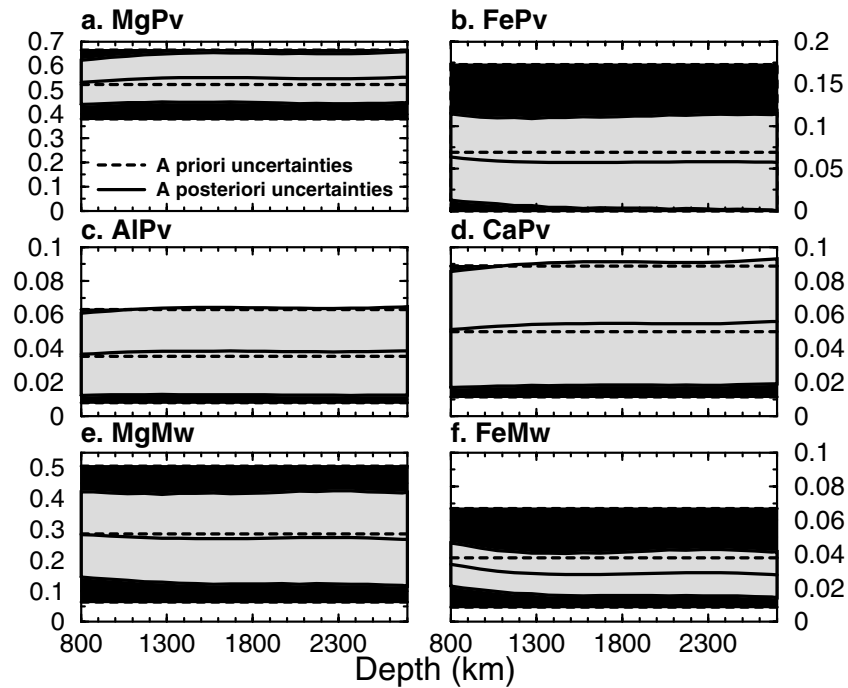


**Figure 4.** Depth dependence of inverted molar fractions of individual end-members:  $MgSiO_3$  perovskite (MgPv),  $FeSiO_3$  perovskite (FePv),  $Al_2O_3$  perovskite (AlPv),  $CaSiO_3$  perovskite (CaPv), periclase (MgMw) and wustite (FeMw). The *a priori* model is pyrolite composition and the geotherm of Brown & Shankland (1981). Shaded areas depict their *a priori* and *a posteriori* uncertainties (light and dark grey shading). Iron-bearing end-members are better constrained than others. Aluminium and calcium perovskite are poorly resolved by the joint inversion of  $\rho$  and  $V_\phi$ .

### 4.3 Influence of *a priori* composition

Since several different models for bulk composition have been proposed, we have also tested the influence of *a priori* composition models on the inverted parameters. We have chosen two additional

*a priori* compositions of the lower mantle that are often discussed. First, a chondritic model (CI carbonaceous chondrite from McDonough & Sun 1995), denoted here as model M2, and second, a model for the lower mantle derived from cosmic abundance analysis by Anderson & Bass (1986), denoted here as model M3. Inverted

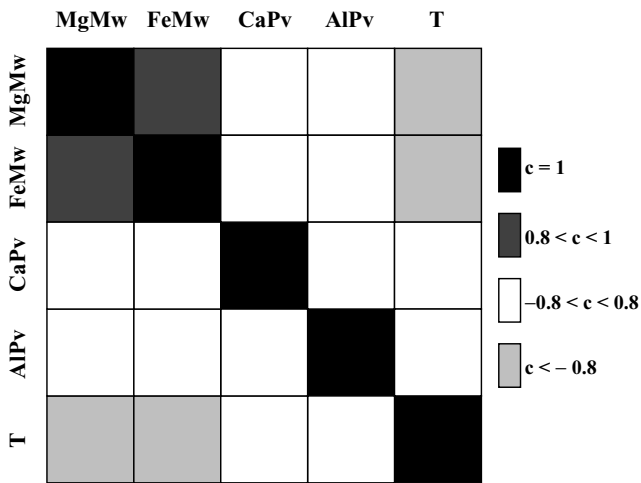


**Figure 5.** Normalized coefficients  $c$  of the correlation matrix between inverted end-members: periclase (MgMw), wustite (FeMw), CaSiO<sub>3</sub> perovskite (CaPv), Al<sub>2</sub>O<sub>3</sub> perovskite (AlPv) molar abundances and temperature (T). The two oxide end-members (MgMw and FeMw) are strongly correlated and anticorrelated with temperature. This matrix is only computed for the independent parameters of our inversion. MgSiO<sub>3</sub> perovskite (MgPv) is fixed through elemental conservation and FeSiO<sub>3</sub> perovskite (FePv) is linked to other parameters via  $K_D$ . The trade-off between MgPv and other parameters is also highlighted in Figs 6 and 7. The values are taken in the mid-mantle when the *a priori* model M1, pyrolite composition and the geotherm of Brown & Shankland (1981), is inverted.

profiles are depicted in Fig. 6 and associated average parameters are summarized in Table 4. As previously observed for the pyrolite M1 model, the most sensitive parameters for the two new models M2 and M3 are also  $X_{Fe}$  and temperature. Therefore the inversion tends to preferentially modify these two values to minimize the misfit function, whereas  $X_{Pv}$  and  $X_{Ca}$  remain close to their original values (that is M2 or M3).

Inversion of the two additional compositions M2 and M3 also reveals the peculiar behaviour of  $X_{Fe}$  down to 1300 km depth. The progressive depletion in iron is again associated with a strongly sub-adiabatic temperature profile. This result seems to support the idea that the gradient of iron content as well as subadiabatic temperature is related to a higher velocity gradient in seismic profiles. In the case of the inverted chondritic model, one observes a decrease of temperature by 150 K between 800 and 1200 km depth. In the mid-mantle, all three geotherms have almost the same adiabatic gradient. The absolute values of temperature are, however, very different. At 1800 km depth, we find 2000 K for the inverted pyrolite model, 2300 K for the inverted chondritic model and 2600 K for the inverted cosmic model. At the base of the mantle, the best-fitting geotherms flatten.

Fig. 6 highlights the trade-off between  $X_{Pv}$  and temperature. A highly perovskitic lower mantle can be reconciled with observed density and bulk sound velocity profiles only if the mantle geotherm is very hot (~2600 K), whereas pyrolitic values of  $X_{Pv}$  yield temperatures slightly colder than the geotherm of Brown & Shankland (1981). The inversion of the cosmic M3 composition indeed gives on average an isothermal lower mantle with  $T \sim 2600$  K. Since the *a posteriori* uncertainties on temperature of the M3 model are

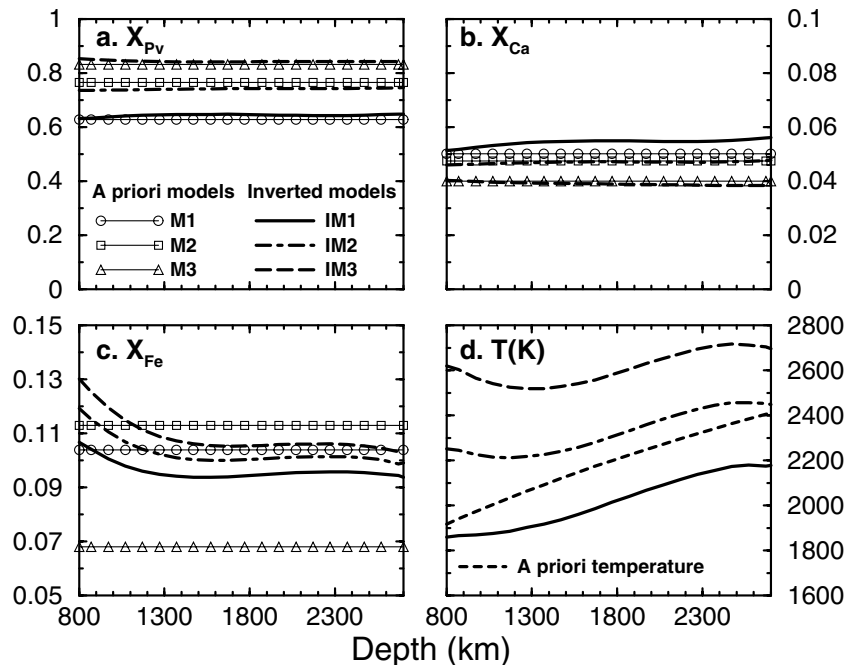


**Figure 6.** Influence of *a priori* compositional model on inverted lower mantle composition (a, b, c) and temperature (d). In all cases, the temperature is inverted from the *a priori* geotherm of Brown & Shankland (1981) (dotted line in d). M1 (circles), *a priori* pyrolite composition (Ringwood 1982); IM1 (solid line), associated inverted model. M2 (squares), *a priori* chondritic CI composition (McDonough & Sun 1995); IM2 (dot-dashed line), associated inverted model. M3 (triangles), *a priori* cosmic composition (Anderson & Bass 1986); IM3 (long dashed line), associated inverted model.  $X_{Fe}$  and temperature are the most sensitive parameters, whereas  $X_{Pv}$  and  $X_{Ca}$  remain close to their *a priori* values. There is a strong positive trade-off between  $X_{Pv}$  and temperature. Seismic density and bulk sound velocity profiles can be explained either by a ‘cold’ (i.e. ~2000 K) pyrolite-like lower mantle ( $X_{Pv} \sim 0.64$ ) or by a ‘hot’ (i.e. ~2600 K) perovskitic lower mantle ( $X_{Pv} \sim 0.84$ ). The resulting uncertainties on temperature profiles do not overlap, making this observation a robust result.

**Table 4.** Average inverted compositions for several *a priori* models and associated estimation of the temperature at the 660 km discontinuity,  $T_{660}$ , and at the core–mantle boundary,  $T_{\text{CMB}}$ . The temperature is inverted and the *a priori* temperature profile is the geotherm of Brown & Shankland (1981), except for model IM1T.

	$X_{\text{Pv}}$	$X_{\text{Ca}}$	$X_{\text{Fe}}$	$T_{660}$ (K)	$T_{\text{CMB}}$ (K)
Pyrolite <sup>a</sup>	0.622	0.051	0.104	1873	2450
IM1	$0.643 \pm 0.172$	$0.054 \pm 0.036$	$0.096 \pm 0.062$	1800	2300
IM1T	$0.687 \pm 0.103$	$0.059 \pm 0.033$	$0.101 \pm 0.027$	–	–
Chondrite CI <sup>b</sup>	0.761	0.048	0.113	1873	2450
IM2	$0.741 \pm 0.174$	$0.047 \pm 0.031$	$0.103 \pm 0.067$	2200	2500
Cosmic <sup>c</sup>	0.830	0.041	0.068	1873	2450
IM3	$0.843 \pm 0.184$	$0.039 \pm 0.025$	$0.109 \pm 0.077$	2500	2700

<sup>a</sup>Ringwood (1982), model M1. IM1, inverted model 1: inverted temperature and composition when pyrolite is the *a priori* composition. IM1T: inverted composition when pyrolite is the *a priori* composition and the temperature is fixed to the geotherm of Brown & Shankland (1981).

<sup>b</sup>McDonough & Sun (1995), model M2.

<sup>c</sup>Anderson & Bass (1986), model M3. IM2 and IM3: inverted models (composition and temperature) associated with *a priori* models M2 and M3, respectively.

~100 K, this hot geotherm can overlap neither the geotherm of Brown & Shankland (1981) nor that inverted from the M1 model, which makes this conclusion robust. In that case, the lower mantle would be chemically and thermally distinct from the upper mantle. This would call for the presence of a pronounced thermal and chemical boundary layer at or near 660 km depth.

#### 4.4 Influence of temperature

The previous inversions indicate that temperature is a sensitive parameter. If the geotherm were known, one could significantly increase the resolution of other parameters. However, there is no general agreement on the thermal regime of the lower mantle. Recent numerical simulations of mantle convection (e.g. Bunge *et al.* 2001) imply that the mantle geotherm is not adiabatic, whereas the usual analysis of the seismological profiles (e.g. PREM and ak135) suggests it is close to an adiabatic profile.

In order to study the influence of various geotherms on our inversion, we perform several numerical experiments where the temperature profile is kept fixed (its covariance is strongly reduced). In other words, we invert for the composition only. We consider the geotherm proposed by Brown & Shankland (1981),  $T_1$ , modified by  $\pm 400$  K, the geotherm extracted from Bunge *et al.* (2001),  $T_2$ , and a strongly superadiabatic profile similar to that discussed by Shankland & Brown (1985),  $T_3$ . Fig. 7 shows that the inverted composition depends on the choice of the geotherm. This is not surprising because the inversion has to modify other less sensitive parameters (such as  $X_{\text{Pv}}$  and  $X_{\text{Ca}}$ ) to match observed density and bulk sound velocity. Variations of  $\pm 400$  K in the adiabat of Brown & Shankland (1981) induce modifications of  $X_{\text{Pv}}$  of 16 per cent, of  $X_{\text{Ca}}$  of 17 per cent and of  $X_{\text{Fe}}$  of 12 per cent (shaded areas in Fig. 7). Although  $X_{\text{Fe}}$  is the most sensitive parameter, due to the correlation with Mg-bearing end-members all changes are not accommodated by  $X_{\text{Fe}}$ . Since the convective geotherm from Bunge *et al.* (2001) is included within the shaded area, the inverted composition does not lie outside those obtained previously. Therefore, a precise evaluation of effects due to imposing subadiabatic gradients is beyond the resolution of our inversion. In these cases, the inverted composition appears to be homogeneous throughout the mantle (except for the peculiar iron behaviour as already mentioned). A gradient of bulk composition is, however, obtained with the superadiabatic profile

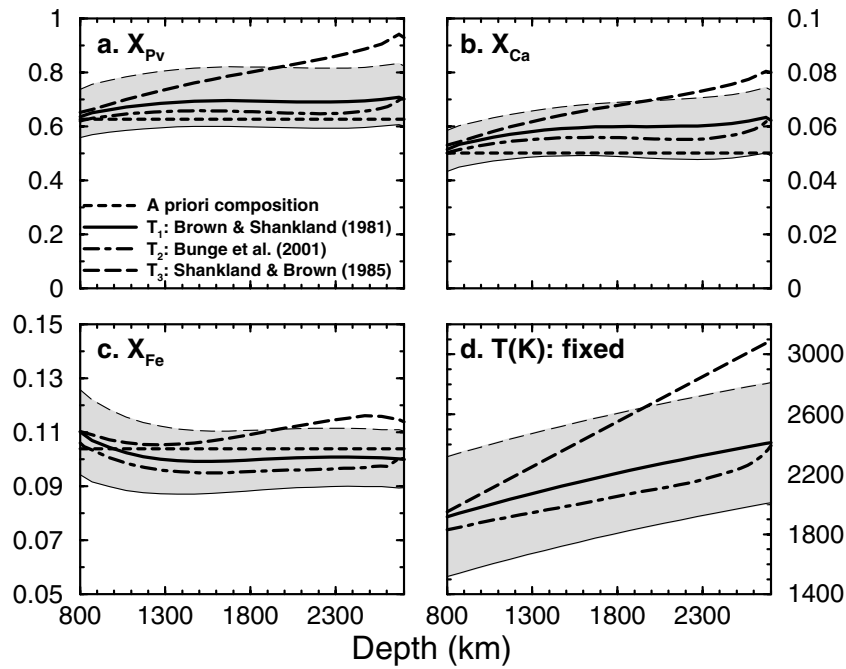
$T_3$ :  $X_{\text{Pv}}$ ,  $X_{\text{Ca}}$  and  $X_{\text{Fe}}$  gradually increase with depth. For example,  $X_{\text{Pv}}$  goes from a pyrolite value at 800 km depth to a value close to 1 at the CMB. Similarly, a gradient of bulk composition is obtained when we assume an isothermal lower mantle.

Fig. 7 reflects the trade-off between  $X_{\text{Pv}}$  and temperature that was discussed in Section 4.3. It also highlights trade-offs between other parameters: hot lower mantle is likely to be consistent not only with high  $X_{\text{Pv}}$  but also with high iron content and high calcium perovskite content. Extrapolating this trend, an entirely perovskitic lower mantle ( $X_{\text{Pv}} + X_{\text{Ca}} = 1$ ) would require a temperature about 900 K higher than the geotherm of Brown & Shankland (1981) and a corresponding iron content of around 0.13. This would lead to a temperature at the 660 km discontinuity close to 2800 K.

#### 4.5 Influence of elastic data

The previous computations have been performed assuming a perfect knowledge of thermodynamic data, i.e. the experimental uncertainties were not considered. However, as discussed in Section 2, some of the EoS parameters of lower mantle minerals remain uncertain (see Table 1). In order to take into account these uncertainties (modelling uncertainties on  $g$ ), we have performed several inversions changing the parameter sets of MgSiO<sub>3</sub> perovskite, Al<sub>2</sub>O<sub>3</sub> perovskite, CaSiO<sub>3</sub> perovskite and periclase.

We first study the effect of the bulk modulus of MgPv. Due to the previously discussed correlations between elastic parameters, we consider the three different confidence ellipses obtained by assuming three values of  $K_{0,T}$  (246, 250 and 261 GPa) as shown in Fig. 1. Inverted composition and temperature profiles are plotted in Fig. 8. The most significant variations are found for temperature and iron content (the two most sensitive parameters): 10 per cent for  $X_{\text{Fe}}$  and almost 200 K for temperature. In the case of  $X_{\text{Pv}}$  and  $X_{\text{Ca}}$ , only small effects are observed (less than 4 per cent). It should be noticed that if we do not use the confidence ellipses, in other words if we do not consider elastic parameters as correlated parameters, but instead if we simply use uncorrelated error bars on  $K_{0,T}$ ,  $(\partial K_{0,T}/\partial T)_P$  and  $\alpha$ , the difference in inverted composition and temperature can be extremely important and significantly increased with depth. In that case, the EoS implied by such deviations is inconsistent with experimental  $P$ – $V$ – $T$  measurements at high pressure and high temperature (predicted densities deviate from experimental values far beyond their error bars).



**Figure 7.** Influence of fixed temperature profile (d) on inverted composition (a, b, c) using pyrolite as an *a priori* composition. In order to study the effect of hot and cold geotherms, the geotherm of Brown & Shankland (1981) ( $T_1$ , solid line) is plotted with error bars of  $\pm 400$  K (shaded area). The cases of a geotherm from convection modelling is taken from Bunge *et al.* (2001) ( $T_2$ , dot-dashed line) and a superadiabatic profile (e.g. Shankland & Brown 1985,  $T_3$ , long-dashed line) are also examined. Fixing the temperature implies significant modifications of all compositional parameters. A hot lower mantle is associated with high values of  $X_{Pv}$ ,  $X_{Ca}$  and  $X_{Fe}$ . A pure perovskitic lower mantle (i.e.  $X_{Pv} + X_{Ca} = 1$ ) would call for a geotherm hotter by  $\sim 900$  K than profile  $T_1$ . The composition is uniform throughout the lower mantle, except for the peculiar behaviour of  $X_{Fe}$  down to  $\sim 1300$  km depth, for geotherms  $T_1$  and  $T_2$ . A non-uniform composition is obtained if the lower mantle is superadiabatic (geotherm  $T_3$ ) and would also be observed if the lower mantle were isothermal.

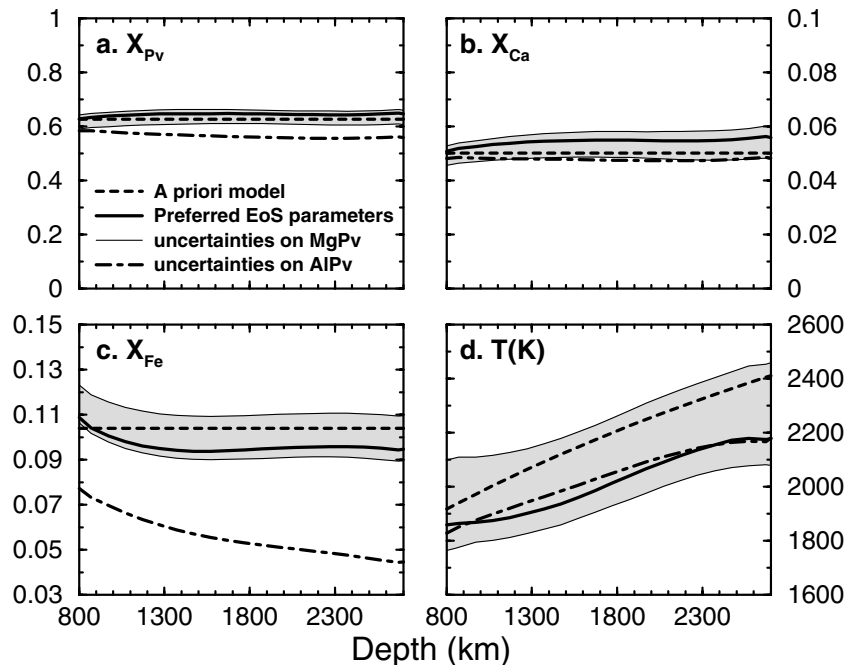


**Figure 8.** Influence of elastic data of MgPv and AlPv on inverted parameters. Uncertainties in the bulk modulus  $K_{0,T}$  of MgPv are considered, using values of 246, 250 and 261 GPa, with associated correlated parameters  $(\partial K_{0,T}/\partial T)_P$  and  $\alpha_0$  within the three ellipses of Fig. 1 (results corresponding to shaded area).  $X_{Fe}$  and temperature are the most sensitive parameters. Equation of state parameters given by Zhang & Weidner (1999) are taken as an alternative extreme set for AlPv (dot-dashed line). This leads to unusual values of  $X_{Fe}$ , decreasing from the top, where  $X_{Fe} \simeq 75$  per cent of the pyrolite value, to the bottom of the lower mantle, where  $X_{Fe}$  reaches the surprisingly low value of  $\sim 0.04$ . The temperature remains within the area resulting from uncertainties in MgPv. Alternative sets for MgMw (Dewaele *et al.* 2000) and for CaPv (Shim *et al.* 2000) give very similar results to those obtained with the preferred elasticity data sets. Despite the fact that considerable attention has been given to experiments on MgPv, the uncertainties still have a significant impact on our conclusions.

Second, we analyse the influence of uncertainties in the bulk modulus of AlPv. As discussed in Section 2, aluminium is thought to decrease the bulk modulus of perovskite, but some studies suggest a much stronger effect than others. We consider the set of elastic parameters given by Zhang & Weidner (1999) as an alternative (extreme) case. The associated results are outside the range of compositions due to uncertainties in the properties of MgPv (Fig. 8). Although the temperature profile obtained with the EoS of Zhang & Weidner (1999) lies within the uncertainties of MgPv,  $X_{\text{Fe}}$  is surprisingly low. The iron content decreases from the top ( $X_{\text{Fe}} = 75$  per cent of pyrolite value) to the bottom of the mantle where  $X_{\text{Fe}}$  is diminished by a factor 2. This behaviour is due to the fact that EoS of Al-bearing perovskite from Zhang & Weidner (1999) differs very significantly from that of MgPv. Indeed, the bulk modulus deduced from Zhang & Weidner (1999) is 20 per cent lower than our preferred value in the mid-mantle ( $K_{0,T} \simeq 420$  GPa instead of 520 GPa). Small uncertainties in the major phase such as MgPv ( $\sim 55$  mol%) have the same effect as large uncertainties in a minor phase such as AlPv ( $\sim 4$  mol%). The final uncertainties in the inverted parameters may be viewed as the combination between uncertainties in Fig. 3 and those in Fig. 8.

We have also verified that the EoS obtained for periclase from Dewaele *et al.* (2000) and for calcium perovskite from Shim *et al.* (2000) give very similar results compared with our preferred set of parameters. This is because both alternative EoS describe almost equally well the high-pressure and high-temperature  $P$ - $V$ - $T$  measurements. Improving the EoS of MgMw and CaPv will affect our results less than further improvements in the EoS of other components.

## 5 DISCUSSION AND CONCLUSION

Fig. 9 shows the relative differences between the computed density and bulk sound velocity, and those given by PREM and ak135, before and after inversion. As required by the *a priori* covariances

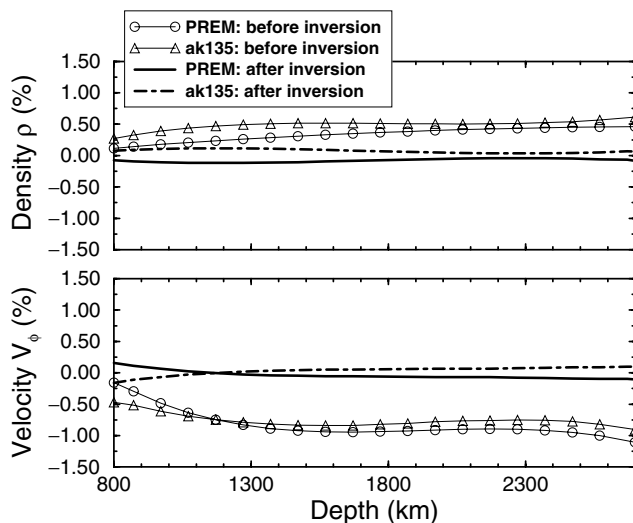


**Figure 9.** Profiles of density ( $\rho$ ) and bulk sound velocity ( $V_{\phi}$ ) before and after inversion. These properties are plotted as residuals relative to the seismic models PREM (Dziewonski & Anderson 1981) and ak135 (Kennett *et al.* 1995). As required by our inversion, the inverted parameters match both PREM and ak135 models, within 0.5 per cent for density and within 0.1 per cent for bulk sound velocity. All the inversions discussed in this paper lead to similar *a posteriori* fits.

(see eq. 1), the inverted parameters match the seismological models within 0.5 per cent for the density and 0.1 per cent for the bulk sound velocity. Although this figure was obtained using pyrolite as an *a priori* model, similar *a posteriori* fits are computed for all the inversions discussed in this paper. This is due to the fact that we are dealing with an under-determined inversion and that at least two model parameters are sufficiently sensitive to the observed data. We have seen in this study that the iron content and the temperature were the most sensitive parameters of the inversion.

Our results support a uniform (but not uniquely defined) chemical composition throughout the lower mantle, except for a peculiar behaviour of iron content down to  $\sim 1300$  km depth. Former studies have also proposed a constant composition with depth for the lower mantle (e.g. Jackson 1998; Marton & Cohen 2002; Deschamps & Trampert 2004), without any anomalous trend for iron. In this study, whatever the *a priori* compositional model (M1, M2 or M3), the inversion changes the most sensitive parameters (temperature and iron content) in order to match seismic profiles (see Table 4). The inverted compositions  $X_{\text{Pv}}$  and  $X_{\text{Ca}}$  are only slightly modified compared with their associated *a priori* models. In all cases, the iron content is found to have very similar values:  $X_{\text{Fe}} = 0.096$  for IM1,  $X_{\text{Fe}} = 0.103$  for IM2 and  $X_{\text{Fe}} = 0.109$  for IM3. The iron content appears to be the most robust feature of the inversion.

We find no clear indication for a deep chemically distinct layer or compositional boundary as proposed by Kellogg *et al.* (1999) and van der Hilst & Kárason (1999). This could be explained by the fact that this layer may undulate in the lower mantle, and may also be associated with small density contrast as suggested by recent numerical experiments (e.g. Cizkova & Matyska 2004). It may be undetectable in 1-D seismic profiles and may therefore not be detected by our inversion. In order to rule out or confirm the existence of such a boundary, the resolution of the inversion needs to be significantly improved by adding other independent observations.

The average geotherm is not very different from an adiabat. In the case of the IM1 model (inverted pyrolite), the resulting temperature profile is colder than the *a priori* geotherm of Brown & Shankland (1981), ranging from  $\sim 1800$  K at the 660 km discontinuity to  $\sim 2300$  K at the core-mantle boundary (within  $\pm 250$  K of uncertainty). The main difference from the geotherm of Brown & Shankland (1981) is the subadiabaticity observed from 660 to 1300 km and above 2500 km. This temperature characteristic is correlated with a decreasing iron down to  $\sim 1300$  km depth. Although these results are biased by large *a posteriori* uncertainties, we obtain the same behaviour in all numerical experiments performed in this study. We have identified this combined behaviour as due to higher velocity gradients present both in PREM and ak135. This could be a signature of multiple phase transitions (some of which may be gradual) below 660 km depth. As previously mentioned, the decomposition of garnets to perovskites can take place over a large region below the 660 km discontinuity (e.g. Hirose *et al.* 1999). Tomographic imaging also reports complex slab morphology in this region (see e.g. Albarède & van der Hilst 2002 for a review). Mantle cross-sections reveal that some subducting slabs do not penetrate immediately into the lower mantle but instead may flatten at the 660 km discontinuity. Since the iron content is significantly higher in basaltic crust than in the surrounding mantle ( $X_{\text{Fe}} \sim 0.5$ , e.g. Hirose *et al.* 1999), slab trapping could lead to an accumulation of iron-enriched material in that depth region. These features can in addition be smeared by seismic observation and by averaging when computing radial profiles. The associated sigmoidal shapes of the geotherms and iron contents in Fig. 6 may also be explained

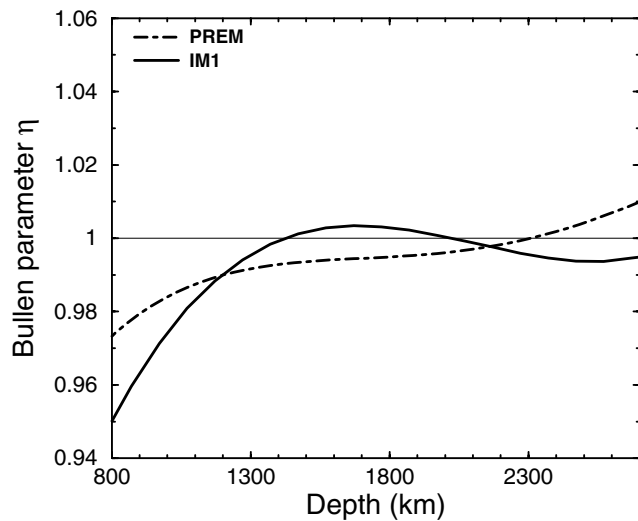


**Figure 10.** Computed Bullen parameter  $\eta$  associated with the inverted lower mantle model IM1 (pyrolite composition and the geotherm of Brown & Shankland (1981) as an *a priori* model). Below 1300 km,  $\eta$  is close to 1, in agreement with a homogeneous and adiabatic lower mantle as discussed in the text. From 800 to 1300 km, it is significantly lower than 1, ranging from 0.95 to 0.99. Since in this region the associated temperature profile is subadiabatic, this is due to iron depletion. Its contribution to  $\eta$  is negative and large enough to counterbalance the positive subadiabatic contribution. Similar Bullen parameters are computed in all the numerical experiments performed in this study.

by the simple polynomial parametrization of the wave speed–depth variation of the PREM model. However, considering ak135 seismic profiles leads to similar but less pronounced trends for  $X_{Fe}$  and temperature gradient. An artefact related to the PREM parametrization has also been reported by Stacey (1997) and Jackson (1998).

The inverted temperature and composition characteristics can also be expressed using the Bullen parameter  $\eta$ . Since it is defined as the ratio between compressibilities of real mantle ( $d\rho/dz$ ) and of a perfectly homogeneous and adiabatic model, the Bullen parameter measures the departure of the mantle from homogeneity and adiabaticity. We have computed  $\eta$  associated with the inverted lower mantle model IM1 (see Fig. 10). Similar values of  $\eta$  were found in all numerical experiments performed in this study. Below 1300 km depth, the Bullen parameter is very close to 1, which is consistent with the homogeneous and adiabatic mantle as already discussed. In the region from 800 to 1300 km, the Bullen parameter is significantly lower than 1, ranging from 0.95 to 0.99. Since the temperature is found to be subadiabatic in this region, this value may seem surprising. Indeed, if the bulk composition is constant, subadiabatic temperature induces  $\eta > 1$ . Values lower than 1 are due to the associated depletion of iron content inferred for this region. Since the iron end-members are always denser than the magnesian end-members, the contribution of non-homogeneity to  $\eta$  is negative and large enough to overcome the positive subadiabatic temperature contribution.

The geotherm is not superadiabatic in any of the numerical experiments. The temperature obtained at the CMB is at most 3300 K (for a lower mantle consisting entirely of perovskite). These conclusions are in contradiction to those obtained by da Silva *et al.* (2000). This is probably because they considered the radial profile of  $K_S$  only and had a significantly different set of elastic parameters. They also kept the chemical composition fixed and tried to match the  $K_S$  seismic profile by changing the temperature alone. However, the generalized

inversion demonstrates that iron content is an equally sensitive parameter and that when it is taken into consideration the temperature profile needs to be modified to a much gentler gradient and lower values. Our temperature profile is also different from that obtained by Deschamps & Trampert (2004). They obtained a superadiabatic profile with a maximum temperature of 3300 K at the CMB. As in the previous case, these differences are probably due to use of a different data set and observational constraints (density, bulk and shear moduli).

This study highlights several important trade-offs between inverted parameters. Fig. 6 demonstrates the positive trade-off between  $X_{Pv}$  and temperature. Seismic density and bulk sound velocity may be equally explained by either a ‘cold’ ( $\sim 2000$  K) pyrolite-like composition or by a ‘hot’ ( $\sim 2600$  K) perovskite-rich composition. This result is robust since the two temperature profiles do not overlap within their *a posteriori* uncertainties. Similar conclusions have been reported in previous studies (e.g. Stixrude *et al.* 1992; Jackson 1998; Marton & Cohen 2002; Deschamps & Trampert 2004). Fig. 7 shows that a hot geotherm is also associated with a high calcium perovskite content as well as a high iron ratio. A hot lower mantle would imply the existence of a thermal and chemical boundary between the lower and the upper mantle and would favour layered convection. To discriminate between different models from radial profiles, more accurate independent observations such as shear properties are required. Since the latter also seem to be more sensitive to the presence of minor elements (Karki & Crain 1998; Jackson *et al.* 2004), they should help to constrain not only temperature but also abundances of calcium and aluminium.

Despite taking particular care in selecting elastic parameters, *a posteriori* uncertainties resulting from uncertainties in the elasticity database remain large. The inverted composition and temperature are sensitive to the selected data. We believe that differences in conclusions between most previous studies result from different choices of elastic parameters. It is therefore inappropriate to directly compare results from various studies without checking their database. Although MgPv is about ten times more abundant than AlPv, the inaccuracy of the EoS of AlPv, especially of its  $(\partial K_{0,T}/\partial T)_P$  and  $\alpha$ , is a dominant source of uncertainties. It should be noticed that we have also tested the influence of various models when averaging  $K_S$  (Reuss, Voigt or Reuss–Voigt–Hill average).  $X_{Pv}$  and  $X_{Ca}$  are not sensitive to this averaging. Assuming a Voigt average instead of a Hill average leads to an iron content higher by 7 per cent and a temperature higher by at most 150 K. The resulting uncertainties are, however, of lesser importance than those induced by inaccuracy of the EoS of MgPv.

We demonstrate that the iron partitioning coefficient is not a crucial parameter in constraining the lower mantle composition and temperature since the resulting inverted parameters do not depend on the value of  $K_D$ . What is indeed important is the total iron content and not the distribution of this element between perovskite and magnesiowustite. This can be explained by the fact that a moderate iron content has a small effect on thermoelastic properties. This result *a posteriori* validates our choice of an ideal solid solution model as well as our choice of calorimetric data ( $\Delta H_f^0$ ,  $S_0$  and  $C_P$ ) for perovskite and magnesiowustite. A more sophisticated solid solution model seems unnecessary. Even an extreme  $K_D$  variation within the lower mantle (Badro *et al.* 2003) would not significantly change our conclusions. This conclusion will, however, not be valid if observations sensitive to iron partitioning are used, as may be the case for shear properties, or if iron significantly affects the bulk modulus of perovskite (as suggested by Andrault *et al.* 2001).

Indeed, the results of our numerical experiments show the great potential value of incorporating shear properties into the inversion for mantle properties (see comparison with Deschamps & Trampert 2004 above). They could potentially give additional constraints on the inversion features and, for example, could confirm or rule out the peculiar behaviour of iron and temperature at the top of the lower mantle. Shear properties may also be more sensitive to minor elements. As mentioned earlier, Karki & Crain (1998) have proposed that analysis of the shear properties of  $\text{CaSiO}_3$  perovskite can be used to constrain the abundance of calcium in the lower mantle. Aluminium and iron seem to have a significant effect on shear properties (Kiefer *et al.* 2002; Jackson *et al.* 2004). The complete  $P$ – $T$ – $\mu$  data set for the six lower mantle end-members is not available yet. In order to use high-quality measurements of shear properties for an inverse problem, a careful analysis of the effect of anelastic attenuation (e.g. Karato 1993) is also required. This is beyond the scope of the present paper and will be treated in a forthcoming study.

## ACKNOWLEDGMENTS

We are grateful to François Guyot and Tom Shankland for fruitful discussions. We wish to thank Jeannot Trampert and Ian Jackson for constructive and helpful reviews. This work was partially supported by a collaborative research project between CNRS and the University of Illinois at Urbana-Champaign, and by National Science Foundation grant EAR-0135642 (to JDB).

## REFERENCES

- Aizawa, Y., Yoneda, A., Katsura, T., Ito, E., Saito, T. & Suzuki, I., 2004. Temperature derivatives of elastic moduli of  $\text{MgSiO}_3$  perovskite, *Geophys. Res. Lett.*, **31**(1), L0160, doi:10.1029/2003GL018762.
- Albarède, F. & van der Hilst, R.D., 2002. Zoned mantle convection, *Phil. Trans. R. Soc. Lond., A*, **360**(1800), 2569–2592.
- Allègre, C., Staudacher, T. & Sarda, P., 1986. Rare gas systematics: formation of the atmosphere evolution and structure of the mantle, *Earth planet. Sci. Lett.*, **81**, 127–150.
- Allègre, C., Poirier, J.-P., Humler, E. & Hofmann, A.W., 1995. The chemical composition of the Earth, *Earth planet. Sci. Lett.*, **134**, 515–526.
- Anderson, D.L. & Bass, J.D., 1986. Transition region of the Earth's upper mantle, *Nature*, **320**, 321–328.
- Anderson, O.L. & Hama, J., 1999. Shifts in thermal expansivity with Fe content for solid solutions of  $\text{MgSiO}_3$ – $\text{FeSiO}_3$  with the perovskite structure, *Am. Mineral.*, **84**, 221–225.
- Andraut, D., 2001. Evaluation of (Mg,Fe) partitioning between silicate perovskite and magnesiowustite up to 120 GPa and 2300 K, *J. geophys. Res.*, **106**(B2), 2079–2087.
- Andraut, D., Bolfan-Casanova, N. & Guignot, N., 2001. Equation of state of lower mantle (Al,Fe)- $\text{MgSiO}_3$ , *Earth planet. Sci. Lett.*, **193**, 501–508.
- Angel, R.J., 2001. Equations of state, *Rev. Mineral. Geochem.*, **41**, 35–59.
- Badro, J., Fiquet, G., Guyot, F., Rueff, J.-P., Struzhkin, V.V., Vankó, G. & Monaco, G., 2003. Iron partitioning in Earth's mantle: toward a deep lower mantle discontinuity, *Science*, **300**, 789–791.
- Bass, J.D., Liebermann, R.C., Weidner, D.J. & Finch, S.J., 1981. Elastic properties from acoustic and volume compression experiments, *Phys. Earth planet. Inter.*, **25**, 140–158.
- Bina, C.R. & Silver, P.G., 1997. Constraints on lower mantle composition and temperature from density and bulk sound velocity profiles, *Geophys. Res. Lett.*, **17**, 1153–1156.
- Brodholt, J.P., 2000. Pressure-induced changes in the compression mechanism of aluminous perovskite in the Earth's mantle, *Nature*, **407**, 620–622.
- Brown, J.M. & Shankland, T.J., 1981. Thermodynamic parameters in the Earth as determined from seismic profiles, *Geophys. J. R. astr. Soc.*, **66**, 579–596.
- Bukowinski, M.S.T. & Wolf, G.H., 1990. Thermodynamically consistent decompression: implications for the lower mantle composition, *J. geophys. Res.*, **95**(B8), 12 583–12 593.
- Bullen, K.E., 1975. *The Earth's Density*, Chapman and Hall, London.
- Bunge, H.-P., Ricard, Y. & Matas, J., 2001. Non-adiabaticity in mantle convection, *Geophys. Res. Lett.*, **28**, 879–882.
- Cizkova, H. & Matyska, C., 2004. Layered convection with an interface at a depth of 1000 km: stability and generation of slab-like downwellings, *Phys. Earth planet. Inter.*, **141**, 269–279.
- Coltice, N. & Ricard, Y., 1999. Geochemical observations and one layer mantle convection, *Earth planet. Sci. Lett.*, **174**, 125–137.
- da Silva, C.R.S., Wentzcovitch, R.M., Patel, A., Price, G.D. & Karato, S.-I., 2000. The composition and geotherm of the lower mantle: constraints from the elasticity of silicate perovskite, *Phys. Earth planet. Inter.*, **118**, 103–109.
- Daniel, I., Cardon, H., Fiquet, G., Guyot, F. & Mezouar, M., 2001. Equation of state of Al-bearing perovskite to lower mantle pressure conditions, *Geophys. Res. Lett.*, **28**(19), 3789–3792.
- Daniel, I., Bass, J.D., Fiquet, G., Cardon, H., Zhang, J. & Hanfland, M., 2004. Effects of aluminum on the compressibility of silicate perovskite, *Geophys. Res. Lett.*, **31**, L15608, doi:10.1029/2004GL020213.
- Davaille, A., Le Bars, M. & Carbone, C., 2003. Thermal convection in a heterogeneous mantle, *C.R. Geosci.*, **335**, 141–156.
- Deschamps, F. & Trampert, J., 2004. Towards a lower mantle reference temperature and composition, *Earth planet. Sci. Lett.*, **222**, 161–175.
- Dewaele, A., Fiquet, G., Andraut, D. & Häusermann, D., 2000. P–V–T equation of state of periclase from synchrotron radiation experiments, *J. geophys. Res.*, **105**(B2), 2869–2877.
- Dziewonski, A.M. & Anderson, D.L., 1981. Preliminary reference Earth model, *Phys. Earth planet. Inter.*, **25**, 297–356.
- Fei, Y., 1999. Effects of temperature and composition on the bulk modulus of (Mg,Fe)O, *Am. Mineral.*, **84**, 272–276.
- Fei, Y., Mao, H.-K. & Mysen, B.O., 1991. Experimental determination of element partitioning and calculation of phase relations in the MgO–FeO– $\text{SiO}_2$  system at high pressure and high temperature, *J. geophys. Res.*, **96**(B2), 2157–2169.
- Fei, Y., Wang, Y. & Finger, L.W., 1996. Maximum solubility in (Mg,Fe) $\text{SiO}_3$ –perovskite as a function of temperature at 26 GPa: implications for FeO content in the lower mantle, *J. geophys. Res.*, **101**(B5), 11 525–11 530.
- Ferrachat, S. & Ricard, Y., 2001. Mixing properties in the Earth's mantle: effects of the viscosity stratification and of oceanic crust segregation, *Geochem. Geophys. Geosyst.*, **2**, doi:10.1029/2000GC000092.
- Fiquet, G., Andraut, D., Dewaele, A., Charpin, T., Kunz, M. & Häusermann, D., 1998.  $P$ – $V$ – $T$  equation of state of  $\text{MgSiO}_3$  perovskite, *Phys. Earth planet. Inter.*, **105**, 21–31.
- Fiquet, G., Richet, P. & Montagnac, G., 1999. High-temperature thermal expansion of lime periclase corundum and spinel, *Phys. Chem. Miner.*, **27**, 103–111.
- Fiquet, G., Dewaele, A., Andraut, D., Kunz, M. & Bihan, T.L., 2000. Thermoelastic properties and crystal structure of  $\text{MgSiO}_3$  perovskite at lower mantle pressure and temperature conditions, *Geophys. Res. Lett.*, **27**(1), 21–24.
- Frost, D.J. & Langenhorst, F., 2002. The effect of  $\text{Al}_2\text{O}_3$  on Fe–Mg partitioning between magnesiowustite and magnesian silicate perovskite, *Earth planet. Sci. Lett.*, **199**, 227–241.
- Funamori, N., Yagi, T., Utsumi, W., Kondo, T., Uchida, T. & Funamori, M., 1996. Thermoelastic properties of  $\text{MgSiO}_3$  perovskite determined by in situ X ray observations up to 30 GPa and 2000 K, *J. geophys. Res.*, **101**(B4), 8257–8269.
- Gillet, P., Daniel, I., Guyot, F., Matas, J. & Chervin, J.-C., 2000. A thermodynamic model for  $\text{MgSiO}_3$ –perovskite derived from pressure temperature and volume dependence of the Raman mode frequencies, *Phys. Earth planet. Inter.*, **117**, 361–384.
- Grand, S.P., van der Hilst, R.D. & Widiyantoro, S., 1997. Global seismic tomography a snapshot of convection in the Earth, *GSA Today*, **7**(4), 1–7.
- Green, D.H. & Ringwood, A.E., 1963. Mineral assemblages in a model mantle composition, *J. geophys. Res.*, **68**, 937–945.

- Hama, J. & Suito, K., 1998. Equation of state of MgSiO<sub>3</sub> perovskite and its thermoelastic properties under lower mantle conditions, *J. geophys. Res.*, **103**(B4), 7443–7462.
- Hart, S.R. & Zindler, A., 1986. In search of bulk composition, *Chem. Geol.*, **57**, 247–267.
- Hazen, R.M., 1981. Systematic variation of bulk modulus of wustite with stoichiometry, *Carnegie Inst. Wash. Yearb.*, **80**, 277–280.
- Hirose, K., Fei, Y., Ma, Y. & Mao, H.-K., 1999. The fate of subducted basaltic crust in the Earth's lower mantle, *Nature*, **397**, 53–56.
- Hofmann, A.W., 1997. Mantle geochemistry: the message from oceanic volcanism, *Nature*, **385**, 219–229.
- Irifune, T., 1994. Absence of an aluminous phase in the upper part of the Earth's mantle, *Nature*, **370**, 131–133.
- Irifune, T., Koizumi, T. & Ando, J., 1996. An experimental study of the garnet-perovskite transformation in the system MgSiO<sub>3</sub>-Mg<sub>3</sub>Al<sub>2</sub>Si<sub>3</sub>O<sub>12</sub>, *Phys. Earth planet. Inter.*, **96**, 147–157.
- Isaak, D., Anderson, O. & Goto, T., 1989. Measured elastic moduli of single-crystal MgO up to 1800 K, *Phys. Chem. Miner.*, **16**, 704–713.
- Isaak, D., Cohen, R.E. & Mehl, M.J., 1990. Calculated elastic and thermal properties of MgO at high pressures and temperatures, *J. geophys. Res.*, **95**, 7055–7067.
- Ita, J. & Stixrude, L., 1992. Petrology elasticity and composition of the mantle transition zone, *J. geophys. Res.*, **97**(B5), 6849–6866.
- Ito, E. & Katsura, T., 1989. A temperature profile of the mantle transition zone, *Geophys. Res. Lett.*, **16**, 425–428.
- Jackson, I., 1998. Elasticity composition and temperature of the Earth's lower mantle: a reappraisal, *Geophys. J. Int.*, **134**, 291–311.
- Jackson, I. & Niesler, H., 1982. The elasticity of periclase to 3 GPa and some geophysical implications, in *High Pressure in Geophysics*, pp. 93–113, eds Akimoto, S. & Manghnani, M.H., Center for Academic Publications, Tokyo.
- Jackson, I., Khanna, S.K., Revcolevschi, A. & Berthon, J., 1990. Elasticity shear-mode softening and high-pressure polymorphism of wustite (Fe<sub>1-x</sub>O), *J. geophys. Res.*, **95**(B13), 21 671–21 685.
- Jackson, J.M., Bass, J.D. & Zhang, J., 2004. Sound velocities of aluminous MgSiO<sub>3</sub> perovskite: implications for the Earth's lower mantle, *Geophys. Res. Lett.*, **31**, L10614, doi:10.1029/2004GL019918.
- Jacobsen, S.D., Reichmann, H.-J., Spetzler, H.A., Mackwell, S.J., Smyth, J.R., Angel, R.J. & McCammon, C., 2002. Structure and elasticity of single-crystal (Mg,Fe)O and a new method of generating shear waves for gigahertz ultrasonic interferometry, *J. geophys. Res.*, **107**(B2), doi:10.1029/2001B000490.
- Javoy, M., 1995. The integral enstatite chondrite model of the Earth, *Geophys. Res. Lett.*, **22**(16), 2219–2222.
- Jeanloz, R. & Knittle, E., 1989. Density and composition of the lower mantle, *Phil. Trans. R. Soc. Lond., A*, **328**, 377–389.
- Jeanloz, R. & Sato-Sorensen, Y., 1986. Hydrostatic compression of Fe<sub>1-x</sub>O wustite, *J. geophys. Res.*, **91**, 4665–4672.
- Karato, S.-I., 1993. Importance of anelasticity in the interpretation of seismic tomography, *Geophys. Res. Lett.*, **20**(5), 1623–1626.
- Karki, B.B. & Crain, J., 1998. First-principles determination of elastic properties of CaSiO<sub>3</sub> perovskite at lower mantle pressures, *Geophys. Res. Lett.*, **25**(14), 2741–2744.
- Katsura, T. & Ito, E., 1996. Determination of Fe–Mg partitioning between perovskite and magnesiowustite, *Geophys. Res. Lett.*, **23**(16), 2005–2008.
- Kellogg, L.H., Hager, B.H. & van der Hilst, R.D., 1999. Compositional stratification in the deep mantle, *Science*, **283**, 1881–1884.
- Kennett, B.L.N., Engdahl, A.R. & Buland, R., 1995. Constraints on seismic velocities in the Earth from traveltimes, *Geophys. J. Int.*, **122**, 108–124.
- Kesson, S.E., Fitzgerald, J.D. & Shelley, J.M., 1998. Mineralogy and dynamics of a pyrolite lower mantle, *Nature*, **393**, 252–255.
- Kiefer, B., Stixrude, L. & Wentzcovitch, R.M., 2002. Elasticity of (Mg,Fe)SiO<sub>3</sub>-perovskite at high pressures, *Geophys. Res. Lett.*, **29**(11), 1539 doi:10.1029/2002GL014683.
- Knittle, E. & Jeanloz, R., 1987. Synthesis and equation of state of (Mg,Fe)SiO<sub>3</sub> perovskite to over 100 gigapascals, *Science*, **235**, 668–670.
- Kung, J., Li, B., Weidner, D.J., Zhang, J. & Liebermann, R.C., 2002. Elasticity of (Mg<sub>0.83</sub>Fe<sub>0.17</sub>)O ferropericlase at high pressure: ultrasonic measurements in conjunction with X-radiation techniques, *Earth planet. Sci. Lett.*, **203**, 557–566.
- Lay, T., Williams, Q. & Garnero, E.J., 1998. The core-mantle boundary layer and deep Earth dynamics, *Nature*, **392**, 461–468.
- Liu, M. & Liu, L., 1987. Bulk moduli of wustite and periclase: a comparative study, *Phys. Earth planet. Inter.*, **45**, 273–279.
- Mao, H.-K., Hemley, R.J., Fei, Y., Shu, J.F., Chen, L.C., Jephcoat, A.P., Wu, Y. & Bassett, W.A., 1991. Effect of pressure temperature and composition on lattice parameters and density of (Fe,Mg)SiO<sub>3</sub>-perovskites to 30 GPa, *J. geophys. Res.*, **96**(B5), 8069–8079.
- Mao, H.-K., Shen, G. & Hemley, R.J., 1997. Multivariable dependence of Fe–Mg partitioning in the lower mantle, *Science*, **278**, 2098–2100.
- Martinez, I., Wang, Y., Guyot, F., Liebermann, R.C. & Doukhan, J.-C., 1997. Microstructures and iron partitioning in (Mg,Fe)SiO<sub>3</sub> perovskite-(Mg,Fe)O magnesiowustite assemblages: an analytical transmission electron microscopy study, *J. geophys. Res.*, **102**(B3), 5265–5280.
- Marton, F. & Cohen, R.E., 2002. Constraints on the lower mantle composition from molecular dynamics simulations of MgSiO<sub>3</sub> perovskite, *Phys. Earth planet. Inter.*, **134**, 239–252.
- McDonough, W.F. & Sun, S.-S., 1995. The composition of the Earth, *Chem. Geol.*, **120**, 223–253.
- Monnereau, M. & Yuen, D.A., 2002. How flat is the lower-mantle temperature gradient?, *Earth planet. Sci. Lett.*, **202**, 171–183.
- Parise, J.B., Wang, Y., Yeganeh-Haeri, A., Cox, D.E. & Fei, Y., 1990. Crystal structure and thermal expansion of (Mg,Fe)SiO<sub>3</sub> perovskite, *Geophys. Res. Lett.*, **17**(12), 2089–2092.
- Ricard, Y., Richards, M.A., Lithgow-Bertelloni, C. & Stunff, Y.L., 1993. A geodynamic model of mantle density heterogeneity, *J. geophys. Res.*, **98**, 21 895–21 909.
- Richards, M.A. & Hager, B.H., 1984. Geoid anomalies in a dynamic Earth, *J. geophys. Res.*, **89**, 5987–6002.
- Ringwood, A.E., 1962a. A model for the upper mantle, *J. geophys. Res.*, **67**, 857–867.
- Ringwood, A.E., 1962b. A model for the upper mantle 2, *J. geophys. Res.*, **67**, 4473–4477.
- Ringwood, A.E., 1979. *Origin of the Earth and Moon*, Springer, New York.
- Ringwood, A.E., 1982. Phase transformations and differentiation in subducted lithosphere: implications for mantle dynamics basalt petrogenesis and crustal evolution, *J. Geol.*, **90**(6), 611–642.
- Saxena, S.K., Dubrovinsky, L.S., Tutti, F. & Bihan, T.L., 1999. Equation of state of MgSiO<sub>3</sub> with the perovskite structure based on experimental measurement, *Am. Mineral.*, **84**, 226–232.
- Shankland, T.J. & Brown, J.M., 1985. Homogeneity and temperatures in the lower mantle, *Phys. Earth planet. Inter.*, **38**, 51–58.
- Shim, S.-H., Duffy, T.S. & Shen, G., 2000. The equation of state of CaSiO<sub>3</sub> perovskite to 108 GPa at 300 K, *Phys. Earth planet. Inter.*, **120**, 327–338.
- Silver, P.G., Carlson, R.W. & Olson, P., 1988. Deep slabs geochemical heterogeneity and large-scale structure of mantle convection: investigation of an enduring paradox, *Ann. Rev. Earth planet. Sci.*, **16**, 477–541.
- Sinelnikov, Y.D., Chen, G., Neuville, D.R., Vaughan, M.T. & Liebermann, R.C., 1998. Ultrasonic shear wave velocities of MgSiO<sub>3</sub> perovskite at 8 GPa and 800 K and lower mantle composition, *Science*, **281**, 677–679.
- Sinogeikin, S.V. & Bass, J.D., 2000. Single-crystal elasticity of pyrope and MgO to 20 GPa by Brillouin scattering in the diamond cell, *Phys. Earth planet. Inter.*, **126**, 43–62.
- Sinogeikin, S.V., Jackson, J.M., O'Neill, B., Palko, J.W. & Bass, J.D., 2000. Compact high-temperature cell for Brillouin scattering measurements, *Rev. Sci. Instrum.*, **71**(1), 201–206.
- Sinogeikin, S.V., Zhang, J. & Bass, J.D., 2004. Elasticity of MgSiO<sub>3</sub> polycrystalline perovskite by Brillouin spectroscopy, *Geophys. Res. Lett.*, **31**, L06620, doi:10.1029/2004GL019559.
- Skinner, B., 1966. Thermal expansion, in *Handbook of Physical Constants*, Geological Society of America Memoir, pp. 75–95, ed. Clark, S.P. Jr, Geological Society of America, Boulder, CO.

- Spear, F.S., 1995. Activity models for phases of petrologic importance, in *Metamorphic Phase Equilibria and Pressure-Temperature-Time Paths*, Mineralogical Society of America Monograph, pp. 175–239, Mineralogical Society of America, Washington, DC.
- Stacey, F.D., 1997. Bullen's seismological homogeneity parameter,  $\eta$ , applied to a mixture of minerals: the case of the lower mantle, *Phys. Earth planet. Inter.*, **99**, 189–193.
- Stacey, F.D., 1998. Thermoelasticity of a mineral composite and a reconsideration of lower mantle properties, *Phys. Earth planet. Inter.*, **106**, 219–236.
- Stacey, F.D. & Isaak, D.G., 2001. Compositional constraints on the equation of state and thermal properties of the lower mantle, *Geophys. J. Int.*, **146**, 143–153.
- Stixrude, L., Hemley, R.J., Fei, Y. & Mao, H.K., 1992. Thermoelasticity of silicate perovskite and magnesiowustite and stratification of the Earth's mantle, *Science*, **257**, 1099–1101.
- Sumino, Y., Kumazawa, M., Nishizawa, O. & Pluschkell, W., 1980. The elastic constants of single-crystal  $\text{Fe}_{1-x}\text{O}$  MnO and CoO and the elasticity of stoichiometric magnesiowustite, *J. Phys. Earth*, **28**, 475–495.
- Suzuki, I., 1975. Thermal expansion of periclase and olivine and their anharmonic properties, *J. Phys. Earth*, **23**, 145–159.
- Tackley, P.J., 2000. Mantle convection and plate tectonics: toward an integrated physical and chemical theory, *Science*, **288**, 2002–2007.
- Takafuji, N., Yagi, T., Miyajima, N. & Sumita, T., 2002. Study on  $\text{Al}_2\text{O}_3$  content and phase stability of aluminous- $\text{CaSiO}_3$  perovskite at high pressure and temperature, *Phys. Chem. Miner.*, **29**, 532–537.
- Tarantola, A., 1987. *Inverse Problem Theory. Methods for Data Fitting and Model Parameter Estimation*, Elsevier Science, Amsterdam.
- Tarantola, A. & Valette, B., 1982. Generalized nonlinear inverse problems solved using the least squares criterion, *Rev. Geophys. Space Phys.*, **20**(2), 219–232.
- Utsumi, W., Funamori, N., Yagi, T., Ito, E., Kikegawa, T. & Shimomura, O., 1995. Thermal expansivity of  $\text{MgSiO}_3$  perovskite under high pressures up to 20 GPa, *Geophys. Res. Lett.*, **22**(9), 1005–1008.
- Utsumi, W., Weidner, D.J. & Liebermann, R.C., 1998. Volume measurements of MgO at high pressures and high temperatures, in *Properties of Earth and Planetary Materials at High Pressure and Temperature*, AGU Geophysical Monograph 101, pp. 327–333, eds Manghnani, M.H. & Yagi, T., American Geophysical Union, Washington, DC.
- Vacher, P., Mocquet, A. & Sotin, C., 1998. Computation of seismic profiles from mineral physics: the importance of the non-olivine components for explaining the 660 km depth discontinuity, *Phys. Earth planet. Inter.*, **106**, 275–298.
- van der Hilst, R.D. & K arason, H., 1999. Compositional heterogeneity in the bottom 1000 kilometers of Earth's mantle: toward a hybrid convection model, *Science*, **283**, 1885–1888.
- van der Hilst, R.D., Widiyantoro, S. & Engdahl, E.R., 1997. Evidence for deep mantle circulation from global tomography, *Nature*, **386**, 578–584.
- Wang, Y. & Weidner, D.J., 1994. Thermoelasticity of  $\text{CaSiO}_3$  perovskite and implications for the lower mantle, *Geophys. Res. Lett.*, **21**(10), 895–898.
- Wang, Y., Weidner, D.J., Liebermann, R.C. & Zhao, Y., 1994. P-V-T equation of state of (Mg,Fe)SiO<sub>3</sub> perovskite: constraints on composition of the lower mantle, *Phys. Earth planet. Inter.*, **83**, 13–40.
- Wang, Y., Weidner, D.J. & Guyot, F., 1996. Thermal equation of state of  $\text{CaSiO}_3$  perovskite, *J. geophys. Res.*, **101**(B1), 661–672.
- Watt, J.P., Davies, G.F. & O'Connell, J., 1976. The elastic properties of composite minerals, *Rev. Geophys. Space Phys.*, **14**, 541–563.
- Webb, S. & Jackson, I., 2003. Anelasticity and microcreep in polycrystalline MgO at high temperature: an exploratory study, *Phys. Chem. Miner.*, **30**, 157–166.
- Wentzcovitch, R.M., Karki, B.B., Cococcioni, M. & de Gironcoli, S., 2004. Thermoelastic properties of  $\text{MgSiO}_3$  -perovskite: insights on the nature of the Earth's lower mantle, *Phys. Rev. Lett.*, **92**(1), 018501, doi: 10-1103/PhysRevLett.92.018501.
- Will, G., Hinze, E. & Nuding, W., 1980. The compressibility of FeO measured by energy dispersive X-ray diffraction in a diamond anvil squeezer up to 200 kbar, *Phys. Chem. Miner.*, **6**, 157–167.
- Wood, B.J. & Rubie, D.C., 1996. The effect of alumina on phase transformations at the 660-kilometer discontinuity from Fe–Mg partitioning experiments, *Science*, **273**, 1522–1524.
- Yagi, T., Suzuki, T. & Akimoto, S., 1985. Static compression of wustite ( $\text{Fe}_{0.98}\text{O}$ ) to 120 GPa, *J. geophys. Res.*, **90**, 8784–8788.
- Yagi, T., Okabe, K., Nishiyama, N., Kubo, A. & Kikegawa, T., 2004. Complicated effects of aluminum on the compressibility of silicate perovskite, *Phys. Earth planet. Inter.*, **143–144**, 81–91.
- Yamamoto, T., Yuen, D.A., and Ebisuzaki, T., 2003. Substitution mechanism of Al ions in  $\text{MgSiO}_3$  perovskite under high pressure conditions from first-principles calculations, *Earth planet. Sci. Lett.*, **206**, 617–625.
- Yeganeh-Haeri, A., Weidner, D.J. & Ito, E., 1989. Elasticity of  $\text{MgSiO}_3$  in the perovskite structure, *Science*, **243**, 787–789.
- Zhang, J., 2000. Effect of pressure on thermal expansion of MgO up to 8.2 GPa, *Phys. Chem. Miner.*, **27**, 145–148.
- Zhang, J. & Weidner, D.J., 1999. Thermal equation of state of aluminum-enriched silicate perovskite, *Science*, **284**, 782–784.

## APPENDIX A: BULK PROPERTIES OF AN ASSEMBLAGE AT HIGH P AND HIGH T

### Birch–Murnaghan equation of state

We use the Birch–Murnaghan equation of state (third order) to relate pressure  $P$ , temperature  $T$  and volume  $V$  (Bullen 1975):

$$P = \frac{3}{2}K_T \left[ \left( \frac{V_{T,0}}{V} \right)^{7/3} - \left( \frac{V_{T,0}}{V} \right)^{5/3} \right] \times \left\{ 1 - \frac{3}{4}(4 - K'_{0,T}) \left[ \left( \frac{V_{T,0}}{V} \right)^{2/3} - 1 \right] \right\} \quad (\text{A1})$$

where  $K_T$ ,  $K'_{0,T}$  and  $V_{T,0}$  are the isothermal bulk modulus, its pressure derivative and the volume at ambient pressure and temperature  $T$  (in K).  $K'_{0,T}$  is assumed to be a constant.  $K_T$  and  $V_{T,0}$  are obtained from parameters at ambient conditions as follows:

$$K_T = K_{0,T} + \left( \frac{\partial K_{0,T}}{\partial T} \right)_P (T - 298) \quad (\text{A2})$$

$$V_{T,0} = V_0 \exp \left( \int_{298}^T \alpha(T') dT' \right) \quad (\text{A3})$$

where  $K_{0,T}$  and  $V_0$  are the values at ambient conditions ( $P = 1$  bar,  $T = 298$  K), and  $(\partial K_{0,T}/\partial T)_P$  is assumed to be a constant,  $\alpha(T)$  is the thermal expansion at ambient pressure and at temperature  $T$ . We assume a linear dependence of  $\alpha$  with temperature:  $\alpha(T) = \alpha_0 + \alpha_1 T$ .

### Bulk properties of an assemblage

From the molar abundances  $n_i$  of each end-member  $i$ , the molar volume of a lower mantle assemblage is deduced from

$$V = \sum_i n_i V_i, \quad (\text{A4})$$

where  $V_i$  is the partial molar volume of the end-member  $i$ . The other bulk properties are obtained as follows:

(1) Density  $\rho$  from

$$\rho = \frac{1}{V} \sum_i n_i M_i, \quad (\text{A5})$$

where  $M_i$  is the molar weight.

(2) Adiabatic incompressibility  $K_S$  by using its thermodynamic definition, i.e. an incompressibility corresponding to the Reuss average for an assemblage (Watt *et al.* 1976), from

$$K_S = -V \left( \frac{\partial P}{\partial V} \right)_S = V \left( \sum_i n_i \frac{V_i}{K_{S_i}} \right)^{-1}, \quad (\text{A6})$$

where  $K_{S_i}$  is

$$K_{S_i} = K_{T_i} \left( 1 + \frac{\alpha_i^2 V_i K_{T_i} T}{C_{V_i}} \right), \quad (\text{A7})$$

with  $C_{V_i}$  the heat capacity at constant volume (see below).

(3) Bulk sound velocity  $V_\phi$  from

$$V_\phi = \sqrt{\frac{K_S}{\rho}}. \quad (\text{A8})$$

### Heat capacity

The thermodynamic equilibrium at pressure  $P$  and temperature  $T$  between the perovskite and magnesiowustite phases is defined by eq. (7) in the Section 4.1. It requires the computation of the standard chemical potentials  $\mu_i^0(P, T)$  at pressure  $P$  and temperature  $T$  of each end-member  $i$ . The heat capacity of each end-member is needed to compute each  $\mu_i^0$  at  $P$  and  $T$ . It is also used to compute the heat capacities at constant volume  $C_V$  via the expression  $C_V = C_P - \alpha^2 V K_T T$ .